Global Biogeochemical Cycles®

RESEARCH ARTICLE
10.1029/2022GB007672

Quantifying Net Community Production and Calcification at Station ALOHA Near Hawai'i: Insights and Limitations From a Dual Tracer Carbon Budget Approach

Lucie A. C. M. Knor[1], Christopher L. Sabine[1], Adrienne J. Sutton[2], Angelicque E. White[1], James Potemra[1], and Robert A. Weller[3]

[1]University of Hawai'i at Mānoa, Honolulu, Hawai'i, USA, [2]NOAA Pacific Marine Environmental Laboratory, Seattle, WA, USA, [3]Woods Hole Oceanographic Institution, Woods Hole, MA, USA

Key Points:

- First calculation of community calcification with a budget approach at this location, results exceed reported sediment trap data
- Independently constrained horizontal and vertical transport of dissolved inorganic carbon/total alkalinity. Largest annual supply: lateral inputs with strong eddy contribution
- It is important to better characterize the physical, especially horizontal, transport of carbon to further investigate mixed layer carbon cycling

Supporting Information:

Supporting Information may be found in the online version of this article.

Correspondence to:

L. A. C. M. Knor,
luciek@hawaii.edu

Citation:

Knor, L. A. C. M., Sabine, C. L., Sutton, A. J., White, A. E., Potemra, J., & Weller, R. A. (2023). Quantifying net community production and calcification at station ALOHA near Hawai'i: Insights and limitations from a dual tracer carbon budget approach. *Global Biogeochemical Cycles*, *37*, e2022GB007672. https://doi.org/10.1029/2022GB007672

Received 11 DEC 2022
Accepted 21 JUN 2023

Author Contributions:

Conceptualization: Lucie A. C. M. Knor, Christopher L. Sabine
Data curation: Lucie A. C. M. Knor, Adrienne J. Sutton, Robert A. Weller
Formal analysis: Lucie A. C. M. Knor
Funding acquisition: Christopher L. Sabine, Adrienne J. Sutton, Angelicque E. White, James Potemra, Robert A. Weller
Investigation: Adrienne J. Sutton

Abstract A budget approach is used to disentangle drivers of the seasonal mixed layer carbon cycle at Station ALOHA (A Long-term Oligotrophic Habitat Assessment) in the North Pacific Subtropical Gyre (NPSG). The budget utilizes data from the WHOTS (Woods Hole—Hawaii Ocean Time-series Site) mooring, and the ship-based Hawai'i Ocean Time-series (HOT) in the NPSG, a region of significant oceanic carbon uptake. Parsing the carbon variations into process components allows an assessment of both the proportional contributions of mixed layer carbon drivers and the seasonal interplay of drawdown and supply from different processes. Annual net community production reported here is at the lower end of previously published data, while net community calcification estimates are 4- to 7-fold higher than available sediment trap data, the only other estimate of calcium carbonate export at this location. Although the observed seasonal cycle in dissolved inorganic carbon in the NPSG has a relatively small amplitude, larger fluxes offset each other over an average year. Major supply comes from physical transport, especially lateral eddy transport throughout the year and entrainment in the winter, offset by biological carbon uptake in the spring. Gas exchange plays a smaller role, supplying carbon to the surface ocean between Dec-May and outgassing in Jul-Oct. Evaporation-precipitation (E-P) is variable with precipitation prevailing in the first half and evaporation in the second half of the year. The observed total alkalinity signal is largely governed by E-P with a somewhat stronger net calcification signal in the wintertime.

Plain Language Summary The ocean carbon cycle is a complicated system where chemical compounds react, are moved by ocean physics, altered by organisms, and exchange with CO_2 in the atmosphere. To explore how the ocean will continue to take up CO_2 from the atmosphere and how much will be removed into the deep ocean, we need to know how these processes influence ocean carbon. Here, we investigate them over a year. We create a model from observations of two carbon compounds, together with calculated estimates of processes (evaporation and precipitation, transport through the water, and air-sea exchange) to back out the influence of two important reaction pairs executed by organisms: Photosynthesis and respiration, and calcification and dissolution. Over a year, the surface community at this location near Hawai'i in the Pacific photosynthesizes more than it respires, removing 53 g of CO_2 per square meter. Also, marine calcifiers perform calcification, and our estimates are much higher than previous measurements from sediment traps. Gas exchange and evaporation-precipitation vary with the seasons in opposite directions, and there are carbon inputs from horizontal transport throughout the year and from water column mixing in the winter.

1. Introduction

1.1. Rationale

The biological pumps are a fundamental component of the global carbon cycle driving the transfer of carbon from the atmosphere to the deep ocean (e.g., Kwon et al., 2009; Marinov et al., 2008; Sigman & Boyle, 2000). Multiple surface ocean processes play a role in carbon concentrations and export from the mixed layer, including physical (gas exchange, evaporation and precipitation, advection, and vertical mixing) and biogeochemical processes, namely photosynthesis, respiration, calcification, and dissolution (Figure 1). The interplay of these processes generates the observed variability in dissolved inorganic carbon (DIC) and total alkalinity (TA) concentrations in the surface ocean (e.g., Sarmiento & Gruber, 2006).

Methodology: Lucie A. C. M. Knor, Christopher L. Sabine
Project Administration: Angelicque E. White, James Potemra, Robert A. Weller
Resources: Christopher L. Sabine
Software: Lucie A. C. M. Knor
Supervision: Christopher L. Sabine, Angelicque E. White, James Potemra
Visualization: Lucie A. C. M. Knor
Writing – original draft: Lucie A. C. M. Knor
Writing – review & editing: Christopher L. Sabine, Adrienne J. Sutton, Angelicque E. White, James Potemra

The North Pacific Subtropical Gyre (NPSG) is an essential system to study when looking at global carbon cycling. Spanning an area of 2×10^7 km^2, the NPSG is the largest ecosystem on earth, and a substantial sink for atmospheric CO_2 (Emerson, 2014). Through the Hawai'i Ocean Time-series (HOT) at Station ALOHA (A Long-term Oligotrophic Habitat Assessment), one of the longest running oceanic time-series at >30 years, the considerable complexity of this oligotrophic "ocean desert" has been and continues to be investigated, with a focus on biogeochemical cycling of carbon and nutrients, from various angles. However, the timing and relative importance of drivers of CO_2-carbonate chemistry and export production over a year are still poorly understood (e.g., Karl & Church, 2017; Karl et al., 2021).

Using TA and DIC as tracers, a mass balance of mixed layer carbon production is constructed at Station ALOHA. Both the organic (Net Community Production, NCP) and inorganic (Net Community Calcification, NCC) components of the biological pump are quantified based on the differing stoichiometry of the reactions of interest (Fassbender et al., 2016, 2017). This allows the evaluation of seasonal variability in and functional interactions between the drivers of carbon cycling in the NPSG. Thanks to the abundance of complementary and redundant datasets at this well-studied location, multiple approaches to quantify several of the mass balance terms can be evaluated for consistency. Sensitivity analyses of physical transport terms, evaporation and precipitation, and mixed layer definition can illuminate the limitations of an upper ocean carbon budget at this location with present data resolution in space and time.

1.2. Study Area: Station ALOHA

Station ALOHA is a time-series study site with a sampling radius of 9.66 km (6 nm) at 22°45′N, 158°W in the NPSG, 100 km north of O'ahu, Hawai'i. Since 1988, approximately monthly cruises to Station ALOHA have been executed by the Hawai'i Ocean Time-series (HOT) program, capturing a variety of oceanographic parameters including thermohaline structure, water column chemistry, primary production, plankton community structure, particle export, and currents throughout the water column. Over the past two decades, moorings within Station ALOHA (2004–2007: MOSEAN Hale-Aloha [www.pmel.noaa.gov/co2/story/HALE-ALOHA] and since 2007: WHOTS [www.soest.hawaii.edu/whots/; www.pmel.noaa.gov/co2/story/WHOTS]) have been recording higher-frequency variability of atmospheric and surface ocean pCO_2 (3-hourly), meteorological data, surface and sub-surface currents (from an Acoustic Doppler current profiler (ADCP) and vector measuring current meters (VMCM, Weller and David (1980)), and temperature and salinity in the upper 155 m (from conductivity, temperature, depth sensors (CTDs)). The unique combination and extent of observations at this site have enabled multiple ground-breaking discoveries in oceanography, such as the ubiquity of marine archaea, and including the identification of important patterns influencing carbon biogeochemical cycling (Karl & Church, 2018). The Hawai'i Ocean Time-series is one of the places where the decrease in surface ocean pH due to anthropogenic CO_2 emissions was first clearly documented.

The ocean in the NPSG is persistently oligotrophic throughout the year with a warm, nutrient-depleted surface layer that is largely isolated from the nutrient-rich deeper waters year-round. Seasons referred to here are defined as spring (March-May), summer (June-August), fall (September-November) and winter (December-February). The sea surface temperature only varies by about 4–5°C seasonally (e.g., Brix et al., 2004). The mixed layer is relatively shallow year-round, between 20 and 120 m (Karl & Lukas, 1996), and the average Mixed layer depth (MLD) changes between ≈30 and 40 m in the summer-fall and ≈70–90 m in the winter.

Part of the declared goals of the Hawaii Ocean Time-series is to explore "*(a) The linkages between seasonal, interannual and long-term (…) variability and trends in ocean physics, chemistry, and biology. (b) Processes underlying physical and biogeochemical temporal variability. (c) The role of physical forcing on carbon fluxes, including rates of biologically mediated carbon transformations, air-sea CO_2 exchange, and carbon export.*" (Church et al., 2013). Many researchers have conducted studies on the carbon cycle at Station ALOHA, mainly in the 1990s and early 2000s (e.g., Brix et al., 2004, 2006; Dore et al., 2003, 2009; Karl et al., 1996; Keeling et al., 2004; Letelier et al., 2000; Neuer et al., 2002; Quay & Stutsman, 2003; Winn et al., 1994, 1998). These studies on biology, physics, and especially the CO_2-carbonate system, carbon cycling, and biological production at this location provide the groundwork for this study.

Identifying and quantifying the processes at work in the subtropical oligotrophic gyres is difficult because of the very low signal-to-noise ratio in inorganic carbon and associated parameters, and the episodic nature and patchiness of biological variability (Church et al., 2013), and "*structure, mechanisms and controls of the*

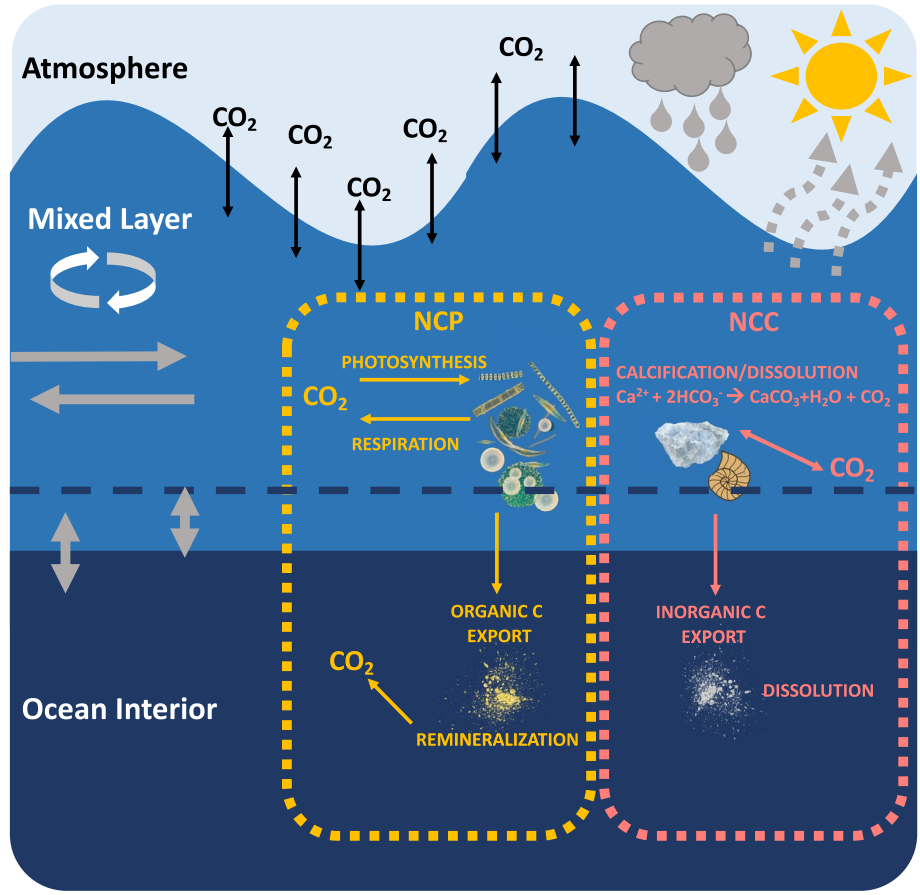

Figure 1. Schematic of processes driving mixed layer carbon cycling. Processes influencing the organic component/net community production (photosynthesis and respiration, yellow) and inorganic component/net community calcification (calcification and dissolution, pink) of the biological carbon pump as well as physical processes (gas exchange, black arrows; evaporation and precipitation, advection, entrainment/detrainment, diffusion, gray arrows).

biological carbon pump at Station ALOHA are not well understood." (Karl & Church, 2017). Brix et al. (2004) report an amplitude of the seasonal salinity-normalized DIC cycle of 15 μmol kg^{-1}, compared to interannual anomalies of 4 μmol kg^{-1}, which suggests that a yearly budget is a good starting point to investigate the drivers of carbon cycling. The seasonal cycle in DIC consists of a summer drawdown in DIC of about 15–20 μmol kg^{-1} between April-September that is attributed to NCP exceeding atmospheric uptake and inputs from physical transport (Keeling et al., 2004; Quay & Stutsman, 2003). NCP has been hypothesized to be the dominant driver for DIC variations over a year (Keeling et al., 2004), but the contributions and timing of other processes remain poorly understood. One of the main difficulties in resolving annual net community production and carbon export with upper ocean mass balance calculations has been the inability to fully constrain relevant lateral and vertical transport terms (Dore et al., 2003; Keeling et al., 2004). We are able to independently constrain all relevant physical transport terms for the first time, thanks to available data from the WHOTS mooring as well as horizontal gradient climatologies from neural networks (Broullón et al., 2019, 2020; Sutton et al., 2014). This allows an evaluation of the relative contribution of processes to the DIC seasonal cycle, and their timing throughout a year. Additionally, a seasonal view of net community calcification is provided for the first time at this location.

2. Data and Methods

2.1. Budget Components

This carbon budget quantifies seasonal climatology from a time-dependent monthly mass balance of carbon (DIC and TA in μmol kg^{-1}) integrated over the mixed layer. It is based on a methodology developed by Fassbender and colleagues (Fassbender et al., 2016, 2017). DIC and TA are used as dual tracers.

Table 1
Summary of Preferred Methodology Used for the Carbon Budget (Method A) and Alternative Approaches for Sensitivity Tests of Individual Terms

Term	Method A	Alternative approaches/sensitivity tests	
Physical Transport: Lateral advection	**Average current, seasonal gradient fit + lateral eddy flux**	WHOTS current climatology, gradient climatology + no eddy flux	Average current, gradient climatology + lateral eddy flux
Physical Transport: Eddy Diffusivity	**Density gradient**	Heat budget	
Evaporation– Precipitation	**Salinity budget**	Meteorological sensors	Salinity normalization
Mixed Layer Depth	**T offset (−0.5°C)**	Density offsets (+0.03 kg m^3, +0.125 kg m^3)	T offset (−1°C)

$$\frac{\partial \mathrm{DIC}}{\partial t} = \left.\frac{\partial \mathrm{DIC}}{\partial t}\right|_{\mathrm{GasEx}} + \left.\frac{\partial \mathrm{DIC}}{\partial t}\right|_{\mathrm{Phys}} + \left.\frac{\partial \mathrm{DIC}}{\partial t}\right|_{\mathrm{Evap,Precip}} + \left.\frac{\partial \mathrm{DIC}}{\partial t}\right|_{\mathrm{Bio}} \quad (1)$$

$$\frac{\partial \mathrm{TA}}{\partial t} = \left.\frac{\partial \mathrm{TA}}{\partial t}\right|_{\mathrm{Phys}} + \left.\frac{\partial \mathrm{TA}}{\partial t}\right|_{\mathrm{Evap,Precip}} + \left.\frac{\partial \mathrm{TA}}{\partial t}\right|_{\mathrm{Bio}} \quad (2)$$

The observed changes in DIC and TA can be decomposed into individual process components that are calculated independently: physical transport, evaporation and precipitation, and for DIC, gas exchange (Equations 1 and 2). With all of the process components and the observed change constrained, the change due to biological processes is determined from the residual. To examine the seasonal changes, monthly averages are used for each term. Monthly averages of the variables are computed for months with >20% data coverage. The physical components of change in DIC and TA over time (gas exchange, evaporation and precipitation (via concentration and dilution of carbon species), horizontal and vertical physical transport) are then evaluated and integrated over the mixed layer.

Finally, the biological term is separated into organic (NCP) and inorganic (NCC) components of biological carbon production, based on stoichiometric ratios from Anderson and Sarmiento (1994). Because organic matter- and calcium carbonate production have different effects on DIC versus TA, we have four equations and four unknowns and can rearrange to explicitly solve for the changes due to NCP and NCC (Equations 3–6). A derivation of these equations can be found in the Supplemental Information of Fassbender et al. (2017). Many of the inputs required for the budget terms are only available as seasonal climatologies, so the results represent average annual cycles. For individual terms, several different methods were tested to evaluate consistency. These approaches are listed in Table 1, and described in detail in the respective sections and the Supporting Information S1. Method A in Table 1 is the preferred methodology.

$$\left.\frac{\partial \mathrm{DIC}}{\partial t}\right|_{\mathrm{NCP}} = \frac{\left(\left.\frac{\partial \mathrm{TA}}{\partial t}\right|_{\mathrm{Bio}} - 2 \times \left.\frac{\partial \mathrm{DIC}}{\partial t}\right|_{\mathrm{Bio}}\right)}{\left(-2 + \frac{-17}{117}\right)} \quad (3)$$

$$\left.\frac{\partial \mathrm{DIC}}{\partial \mathrm{t}}\right|_{\mathrm{NCC}} = \frac{\left.\frac{\partial \mathrm{TA}}{\partial t}\right|_{\mathrm{Bio}} - \left(\frac{-17}{117}\right) \times \left.\frac{\partial \mathrm{DIC}}{\partial t}\right|_{\mathrm{NCP}}}{2} \quad (4)$$

$$\left.\frac{\partial \mathrm{TA}}{\partial \mathrm{t}}\right|_{\mathrm{NCC}} = 2 \times \left.\frac{\partial \mathrm{DIC}}{\partial \mathrm{t}}\right|_{\mathrm{NCC}} \quad (5)$$

$$\left.\frac{\partial \mathrm{TA}}{\partial \mathrm{t}}\right|_{\mathrm{NCP}} = \left(\frac{-17}{117}\right) \times \left.\frac{\partial \mathrm{DIC}}{\partial \mathrm{t}}\right|_{\mathrm{NCP}} \quad (6)$$

2.2. Total Alkalinity and Dissolved Inorganic Carbon

The high temporal resolution time-series from the WHOTS mooring sensors between 2004 and 2021 is of two carbonate system parameters, seawater pCO_2 (pCO_2sw) and pH. However, because the seawater pH record has significant data gaps and pH is not an ideal parameter to pair with pCO_2sw to calculate DIC and TA, we use an alternative approach (McLaughlin et al., 2015; Sutton et al., 2016). To approximate the DIC and TA concentrations at the same temporal resolution, two steps are necessary. First, a regression of salinity and alkalinity from HOT cruise surface data, collected at near-monthly frequency, yields a linear regional salinity-alkalinity relationship. This relationship is then applied to the WHOTS mooring surface salinity time series, which results in a high-resolution alkalinity time-series. From measured pCO_2sw and calculated alkalinity, all CO_2 carbonate system parameters, including DIC, are calculated using the CO2SYS Python package "PyCO2SYS," an adaptation from the MATLAB version (pyco2sys.readthedocs.io; Humphreys, Lewis, et al., 2022; Humphreys, Schiller et al., 2022). Constants used are Sulpis et al. (2020) for carbonic acid and bicarbonate dissociation constants (K_1 and K_2), and Dickson (1990) for K_{SO4}. All other values used are the default terms in the PyCO2SYS package (i.e., default 0 for nutrient concentrations, K_{HF} from Dickson and Riley (1979), and the boron-chlorinity ratio from Uppström (1974)).

A regression of TA and salinity in the top 30 m provided a well-constrained relationship between the two parameters ($R^2 = 0.89$, $n = 630$), and a standard error of the estimate of 4.95 μmol kg^{-1} (Equation 7). The propagated

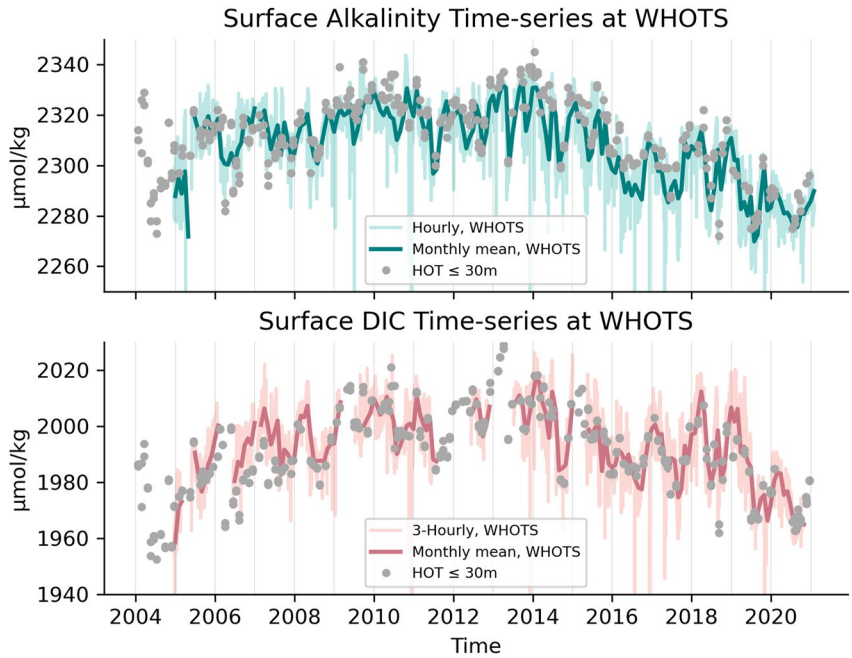

Figure 2. Surface alkalinity and dissolved inorganic carbon time-series at the WHOI Hawaii Ocean Timeseries Station mooring, comparing upper 30 m discrete HOT samples with monthly means from calculated high-resolution (3-hourly) mooring-based data.

error (standard error propagation in CO2SYS) in DIC, calculated from this estimated TA and measured pCO2sw, is 7.7 µmol kg^{-1}. There is good agreement between HOT discrete observations of both TA and DIC with the calculated time-series of these parameters, with mean residuals of +4.0 µmol kg^{-1} for TA (discrete > calculated) and −1.7 µmol kg^{-1} for DIC (discrete < calculated), which fall within the uncertainty estimates (see Figure 2). The somewhat larger offset for TA is due to a difference in salinity measurements from the mooring CTD compared to the shipboard salinity measurements, as salinity is slightly lower in the mooring data. This is probably due to the difference in measurement depth: 0.5 m for the WHOTS mooring compared to 0–30 m for the shipboard CTD.

$$\mathrm{TA} = 66.68 * S - 29.73 \quad (7)$$

2.3. Mixed Layer Depth

Mixed layer depth (MLD) is calculated using a criterion based on a −0.5°C change in temperature relative to the temperature at a 10-m reference depth (Sprintall & Tomczak, 1992). This criterion is one of many that is commonly used at Station ALOHA (e.g., Brix et al., 2004; Keeling et al., 2004). MLD is calculated from the daily average of temperature profiles measured by WHOTS mooring CTD sensors (sampling every minute at 5–10 m spacing) interpolated to a one-m grid. To match the temporal resolution of the budget calculation, the monthly mean of the daily values is used. Visual inspection of all HOT TA and DIC profiles used for the analysis indicated that the −0.5°C temperature threshold most appropriately captures in situ carbon system dynamics compared to other commonly used criteria (see Figure S1 in Supporting Information S1, Movies S1 and S2 for profiles and MLD). To test for sensitivity of the analysis to the MLD definition, a comparison was made to three other MLD definitions: a −1°C temperature threshold (Hastenrath & Merle, 1987) as well as +0.03 kg m^{-3} and +0.125 kg m^{-3} density thresholds (De Boyer Montégut et al., 2004; Levitus, 1982), all relative to a 10-m reference depth.

2.4. Gas Exchange

The contribution of gas exchange to monthly DIC change is calculated using wind speed, SST, salinity, pCO_2air and pCO_2sw data all from WHOTS mooring sensors (Wind speed: http://uop.whoi.edu/currentprojects/WHOTS/whotsarchive.html, CTD: ftp://mananui.soest.hawaii.edu/pub/hot/whots/, pCO_2: Sabine et al., 2012; Sutton et al., 2012), as well as empirical relationships:

Table 2
Terms and Their Units for the Physical Transport Component of the Carbon Budget for Dissolved Inorganic Carbon Are Exactly the Same for Total Alkalinity

Symbol	Quantity	Calculation/source	Units
$\mathbf{u}_{ML}$	Average mixed layer current speed	WHOTS mooring sensors. Mean value from monthly averages over the complete WHOTS time-series.	m/s
DIC	Horizontal DIC/TA climatologies	1° × 1° climatologies based on neural networks from World Ocean Atlas Climatologies (Broullón et al. (2019); Broullón et al. (2020))	μmol/kg
κ_{HOR}	Lateral eddy diffusivity	Zhurbas and Oh (2004).	m^2/s
w_{-h}	Vertical velocity at the ML base	Ekman pumping velocity from ASCAT wind stress curl	m/s
h	Mixed layer depth	−0.5°C temperature offset from 10m reference depth	m
$\frac{\partial DIC}{\partial z}\Big\vert_{z=-h}$	Vertical DIC gradient	HOT profiles of DIC	μmol/kg/m
κ_Z	Eddy diffusivity	Climatology based on density gradients at the base of the mixed layer. Keeling et al. (2004)	m^2/s

$$\left.\frac{\partial \mathrm{DIC}}{\partial t}\right|_{\mathrm{GasExchange}} = \frac{k \times K_H \times \Delta pCO_2}{h} \tag{8}$$

Where k is the piston velocity based on wind speeds at 10m above the surface (Liu et al., 1979), Schmidt number (Wanninkhof, 1992), and a second-order gas transfer parameterization (Ho et al., 2006), and K_H is the CO_2 solubility constant (Weiss, 1974). Details on this calculation are listed in the Supporting Information S1. All measurements are averaged hourly, except for the pCO_2sw and pCO_2air data, which are interpolated linearly to hourly data from measurements taken every 3 hours. Gas exchange is evaluated hourly and then averaged monthly.

2.5. Physical Transport

The physical transport term described for DIC in Equation 9, and exactly the same for TA, comprises horizontal transport, vertical entrainment and diffusion (adapted from Fassbender et al., 2016, 2017). Individual terms and their units are listed below and in Table 2.

$$\left.\frac{\partial \mathrm{DIC}}{\partial t}\right|_{\mathrm{Phys}} = \left.\frac{\partial \mathrm{DIC}}{\partial t}\right|_{\mathrm{Lateral\,transport}} + \left.\frac{\partial \mathrm{DIC}}{\partial t}\right|_{\mathrm{Entrainment}} + \left.\frac{\partial \mathrm{DIC}}{\partial t}\right|_{\mathrm{Diffusion}}$$
$$= \boldsymbol{u}_{\mathrm{ML}} \cdot \nabla \mathrm{DIC} + \kappa_{\mathrm{HOR}} \cdot \nabla^2 \mathrm{DIC} + \left(w_{-h} + \frac{\partial h}{\partial t}\right) \frac{(\mathrm{DIC}_{-h} - \mathrm{DIC}_{\mathrm{ML}})}{h} + \frac{\kappa_z}{h} \left.\frac{\partial \mathrm{DIC}}{\partial z}\right|_{z=-h} \tag{9}$$

2.5.1. Lateral Transport

The complete lateral transport term is calculated as the sum of horizontal background advection, and lateral eddy transport: $\boldsymbol{u}_{\mathrm{ML}} \cdot \nabla \mathrm{DIC} + \kappa_{\mathrm{HOR}} \nabla^2 \mathrm{DIC}$. For background advection, current speeds ($\boldsymbol{u}_{\mathrm{ML}}$) and horizontal gradients in DIC and TA (∇DIC) are required, while the lateral eddy transport is quantified as a lateral eddy diffusivity (κ_{HOR}) times the Laplacian of DIC and TA fields (∇^2DIC).

Horizontal fields of TA and DIC have been quantified elsewhere using multiple linear regression (e.g., Fassbender et al., 2016, 2017) or neural network analysis (e.g., Bittig et al., 2018; Carter et al., 2018). Climatologies around Station ALOHA from a neural network are available for both DIC (Broullón et al., 2020) and TA fields (Broullón et al., 2019). These networks, trained on the GLODAPv2 data set and then applied to World Ocean Atlas (WOA) 2013 climatological data, were tested with Station ALOHA data and proved to be reliable for predicting TA and DIC in this region (Broullón et al., 2019, 2020). They are used here to calculate horizontal gradients and the Laplacian of TA and DIC fields.

Advection was calculated using the overall mean WHOTS velocity in the mixed layer, and the mean plus the annual harmonic fit to the DIC and TA gradients from the Broullón et al. (2019, 2020) climatologies. In situ (WHOTS mooring) current speed measurements are available at high temporal resolution, but horizontal current speeds at this location are dominated by mesoscale eddies (Martínez-Moreno et al., 2022, Figure 3a), which are not resolved by the large-scale (1° × 1°) and long-term seasonal mean TA and DIC fields. An investigation into current speed variability revealed that there is no clear annual cycle (see Figure S3 in Supporting Informa-

tion S1). Therefore, the overall mean current speeds with gradient climatologies best represent the advective component of this budget. The mean zonal component of the current is westward (-0.04 m s^{-1}), and the average meridional current is northward, but barely indistinguishable from zero at 0.008 m s^{-1}. This is consistent with well-established knowledge of large-scale circulation patterns at this location.

In order not to neglect the important contribution of mesoscale eddies (see e.g., Barone et al., 2019), a lateral eddy transport term is added to quantify the influence of the advective component of mesoscale eddies on the tracer budget. An average lateral eddy diffusivity from Zhurbas and Oh (2004) of 8×10^3 m^2 s^{-1} is multiplied by the average divergence of the horizontal gradient field from Broullón et al. (2019, 2020), interpolated to a 2° latitude × 15° longitude grid to reduce noise. For the eddy contribution, a single average value is used throughout the year, while the advective term is at a climatological monthly resolution based on the overall (non-varying) average current speed and an annual harmonic fit of monthly gradient values. An error of 100% is assigned to the lateral eddy transport.

2.5.2. Entrainment and Diffusion

The entrainment term is the flux through the base of the mixed layer, primarily during times of local mixed-layer deepening. The relevant upward vertical velocity component is estimated as monthly mean Ekman pumping from Advanced Scatterometer (ASCAT) daily wind stress curl data (from APDRC: http://www.apdrc.soest.hawaii.edu/) plus changes in MLD over time ($\frac{\partial h}{\partial t}$) (neglecting horizontal advection of the mixed layer gradient). This term is evaluated only for periods of net entrainment; during detrainment, the properties of the water remaining in the mixed layer are not affected by the properties immediately below. Using the sum of these two terms (upward velocity and change over time in MLD), entrainment is then calculated from consecutive HOT cruise profiles in subsequent months and scaled to a monthly value, assuming that the increment of water below the first MLD is mixed into the ML by the time of the following profile. A total of 4 HOT cruise profiles (2%) were excluded due to a mismatch between MLD values and water column DIC/TA data.

As for vertical diffusive transport, DIC and TA vertical gradients across the ML $\left(\frac{\partial \mathrm{DIC}}{\partial z}\Big|_{z=-h}\right)$ are calculated from HOT cruise profiles (again, at near-monthly resolution). The diffusion coefficient or eddy diffusivity (K_z), which governs turbulent diffusion across the bottom of the mixed layer, is not very well constrained due to considerable temporal and spatial variability, and lack of well-resolved measurements (Cronin et al., 2015). It has been established that turbulent diffusion is orders of magnitude higher in the surface mixed layer than in the thermocline below (e.g., Fernández-Castro et al., 2014). Previous budget- or mass-balance-based studies of carbon export at this location often used non-varying, representative K_z values (Table S1 in Supporting Information S1). However, diffusivity has been shown to vary substantially between seasons (e.g., Cronin et al., 2015). Here, we use climatology from Keeling et al. (2004) that was calculated from measurements of the vertical density gradient just below the mixed layer.

The entrainment term is a composite of true monthly averages and near-monthly profiles, while the diffusive term and the lateral eddy transport term are based on climatological values, and hence do not resolve interannual variability. Physical transport contributions can therefore only be evaluated seasonally.

Methods for the sensitivity analysis using alternative approaches (Table 1) for the physical transport term are detailed in the Supporting Information S1 and include using time-varying current speed climatologies from in situ sensors for lateral advection as well as a heat budget calculation adapted from Cronin et al. (2015) for diffusive transport.

2.6. Evaporation—Precipitation

Adapted from Fassbender et al. (2016, 2017), *E–P* is determined as the residual of a mixed layer salinity budget (as in Equation 9), and then scaled to units of μmol kg^{-1} according to Equations 10 and 11. Additionally, evaporation (*E*) and precipitation (*P*) are calculated using two other approaches to evaluate their consistency and sensitivities: A direct *E-P* calculation from meteorological sensors, and salinity normalization are described in the Supporting Information S1.

$$\left.\frac{\partial \mathrm{Sal}}{\partial t}\right|_{E-P} = \frac{\partial \mathrm{Sal}}{\partial t} - \left.\frac{\partial \mathrm{Sal}}{\partial t}\right|_{\mathrm{Phys}} \tag{10}$$

$$\left.\frac{\partial \mathrm{DIC}}{\partial t}\right|_{E-P} = \left.\frac{\partial \mathrm{Sal}}{\partial t}\right|_{E-P} \times \left.\frac{\mathrm{DIC}}{\mathrm{Sal}}\right|_{t=0} \tag{11}$$

Table 3
Error Estimates for Monte Carlo Analysis and Their Sources

Quantity	Error	Source
Total Alkalinity	4.95 µmol kg^{-1}	Standard Error (Equation 11)
DIC	7.7 µmol kg^{-1}	CO2SYS error propagation (Orr et al., 2018)
Temperature	0.002°C	https://geo-matching.com/ctd-systems/37-sm-microcat-c-t-p-recorder)
Salinity	0.012	Measurement uncertainty, Santiago-Mandujano et al. (2016)
pCO_2sw	2 µatm	Measurement uncertainty, Sutton et al. (2014)
pCO_2air	1 µatm	Measurement uncertainty, Sutton et al. (2014)
MLD (h)	2.4 m	¼ of vertical separation of sensors (Fassbender et al., 2016)
Piston velocity (k)	30%	Nightingale et al. (2000), Fassbender et al. (2016)
Wind speed	0.1 m s^{-1}	https://journals.ametsoc.org/view/journals/atot/37/4/jtech-d-19-0132.1.xml
Carbon quotient in Redfield ratio	14	Anderson and Sarmiento (1994)
Turbulent eddy Diffusivity (Kz)	2.2×10^{-5}	Standard deviation of climatological means
Lateral eddy transport	100%	Assigned, since there are no uncertainties reported for K_{LAT}
Mean mixed layer current speeds ($\mathbf{u}_{ML}$)	0.008 m s^{-1}	SEM (from autocorrelation analysis)

2.7. Error Analysis

The error of the linear alkalinity-salinity fit is estimated as the standard error of the estimate (Equation 12). The uncertainty of high-resolution DIC is evaluated using the error propagation tool of CO2SYS (Orr et al., 2018). The uncertainty of each carbon budget term and the final aNCP and aNCC values are evaluated using the Monte Carlo method of error propagation. Each budget term is calculated 1000 times with the input parameters varying according to their uncertainties, assuming a normal distribution. Assigned uncertainties are reported in Table 3.

$$SE = \sqrt{\frac{\sum (TA_{meas} + TA_{calc})^2}{N - 2}} \quad (12)$$

3. Results

3.1. Seasonal Cycle

The seasonal cycle of all budget terms and the observed change are shown in Figure 3. The residual contains all biological processes as well as the errors of all other terms and any processes that are unaccounted for. Mean annual cumulative fluxes in mol C m^{-2} for each term including error estimates are shown in Table 4. Only complete sequential deployment years (July—June) were analyzed for cumulative fluxes, and years with data gaps larger than 1 month were excluded. With uncertainties around 100% for most of the monthly rates of change (see SD in Figure 3), uncertainties for cumulative fluxes range from 80% (for gas exchange) up to 500% (for aNCC).

Table 4
Cumulative Dissolved Inorganic Carbon and Total Alkalinity Fluxes due to Modeled and Calculated Budget Terms in mol C m^{-2} a^{-1}

Term	DIC flux in mol C m^{-2} a^{-1} (mean ± 1SD of Monte Carlo runs)	TA flux in mol C m^{-2} a^{-1} (mean ± 1SD of Monte Carlo runs)
Physical Transport	+2.3 ± 2.6	+1.0 ± 2.1
E–P	– 0.5 ± 1.9	– 0.5 ± 1.9
Gas Exchange	+0.3 ± 0.2	–
Net Community Production	– 0.9 ± 2.8	–
Net Community Calcification	–	– 0.5 ± 2.7

3.1.1. Observed Seasonal Cycle

In an average year, DIC decreases between April-August and increases October–February. TA decreases between February and May, increases between June and October, and stays relatively constant between November and January (Figure 4). There is considerable year-to-year variability in the observed TA and DIC changes each month, indicating that interannual changes in biological and physical processes significantly alter carbon cycling.

3.1.2. Gas Exchange

Gas exchange contributes relatively little to mixed layer DIC variability, with maxima for individual months of +3 and −4 µmol kg^{-1} mo^{-1} (Figure 7a). This corresponds to a climatological maximum CO_2 flux of +4.0 ± 1.2 mmol m^{-2} d^{-1}

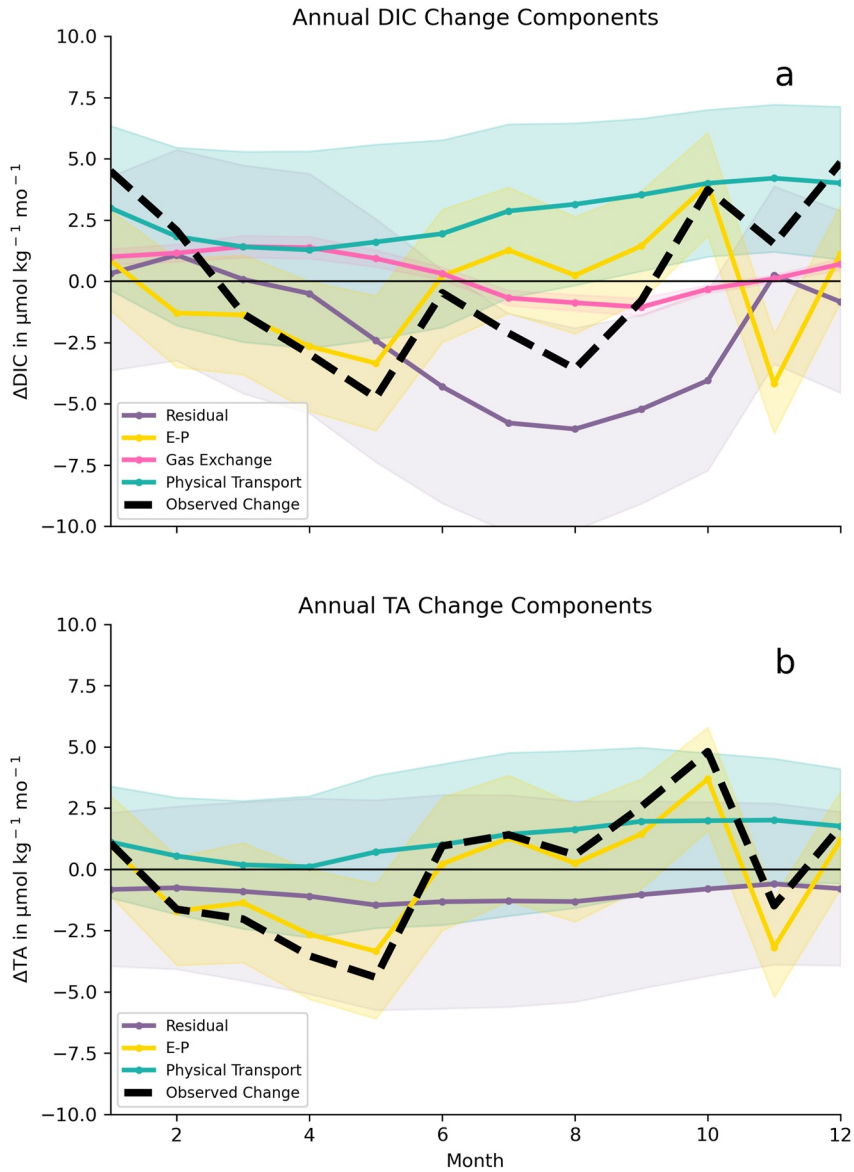

Figure 3. Yearly climatology of the biological term (residual of the budget) and model input terms for dissolved inorganic carbon (3a) and total alkalinity (3b). Shaded areas correspond to ±1 standard deviation of Monte Carlo runs.

for March, and a minimum of -1.6 ± 0.6 mmol m^{-2} d^{-1} in September (data not shown). The seasonal cycle is distinctive, with increasing DIC through December–May (uptake) and decreasing DIC in July–October (outgassing) (Figure 3a), confirming previous studies on time periods of source and sink behavior over the year (e.g., Sutton et al., 2017). The average net annual uptake is 0.34 ± 0.2 mol C m^{-2} from gas exchange at this location.

3.1.3. Evaporation—Precipitation

There is net evaporation between June-October and oscillating positive and negative values for the rest of the year (Figure 3). Cumulative fluxes indicate annual net precipitation (DIC & TA loss), but the associated uncertainty is on the order of 300%.

3.1.4. Physical Transport

DIC changes from physical transport are positive, averaging 2.6 µmol kg^{-1} per month with a maximum of 4.2 ± 2.8 µmol kg^{-1} in November, and a minimum of 1.2 ± 3.7 µmol kg^{-1} in April (Figure 5a). Vertical diffusion supplies small positive inputs throughout the year, and there is a distinctive ~1 µmol kg^{-1} entrainment signal

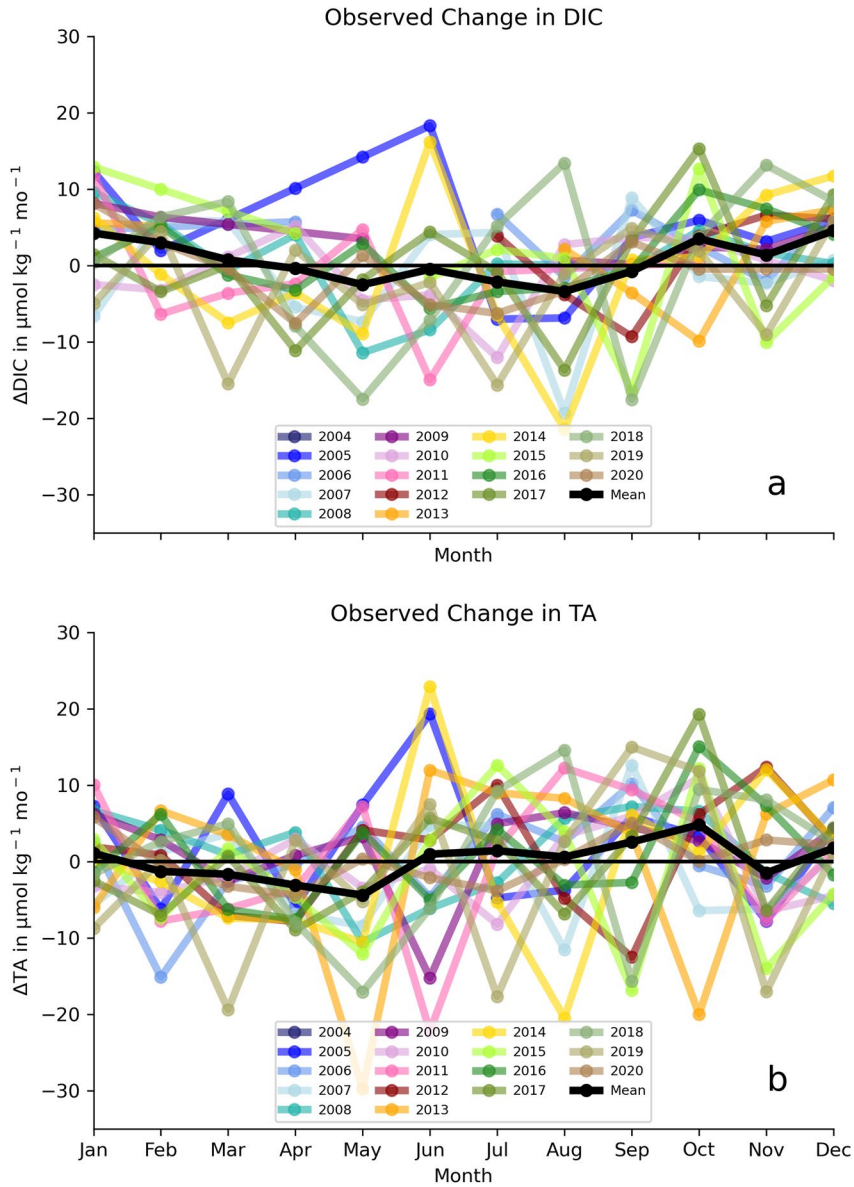

Figure 4. The observed changes in dissolved inorganic carbon (4a) and total alkalinity (4b) each year.

between October-December. There is a seasonal pattern in non-eddy horizontal transport, with the removal of DIC throughout most of the year, as low-DIC waters are advected from the East (and, to a much smaller extent, from the South), except from September-December where fluxes are slightly positive with high-DIC waters advected from the East. The largest contribution in addition to the entrainment signal is the yearly average lateral DIC flux divergence from mesoscale eddies, which is 2 µmol kg^{-1} mo^{-1} (±100%), mainly due to the meridional component of flux divergence. The physical transport term for TA is similar to that of DIC, but smaller (mean: 1.2 µmol kg^{-1} mo^{-1}, maximum: 2.0 ± 2.7 µmol kg^{-1} mo^{-1} September-November) due to both a smaller entrainment peak and a smaller lateral eddy transport term (~1 µmol kg^{-1} mo^{-1}) (Figure 5b).

3.1.5. Biological Term

The residual term for Method A closely matches the observed seasonal DIC cycle (Figure 3a), while the observed TA largely tracks the *E–P* term (Figure 3b), stressing the importance of concentration/dilution for TA and of biological processes for DIC over an annual cycle. The strong DIC drawdown from biological productivity and excess precipitation in the spring is balanced by DIC supply from physical transport and ingassing. A secondary peak in drawdown in the later summer is also opposed by a larger positive physical transport input as well as

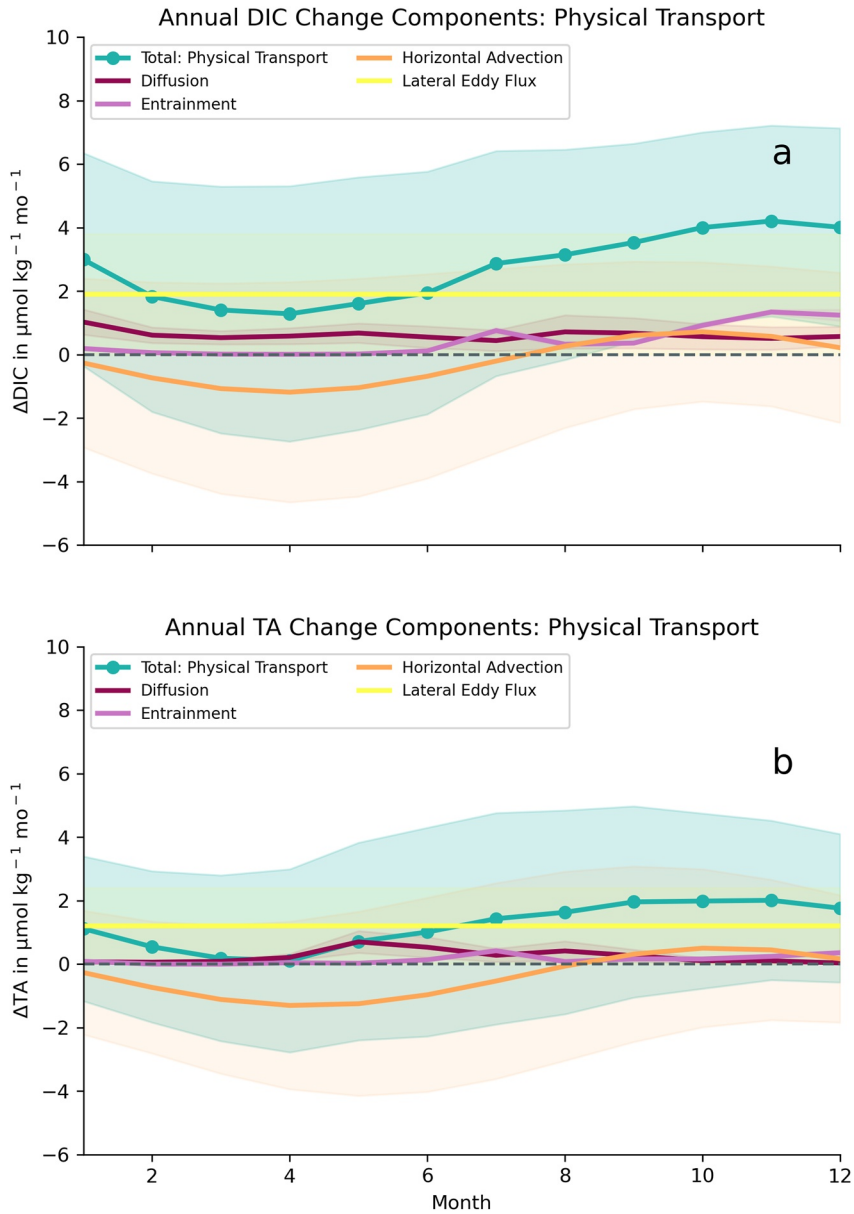

Figure 5. Yearly climatology of the physical transport term and its components for dissolved inorganic carbon (5a) and total alkalinity (5b). Shaded areas correspond to ±1 standard deviation of Monte Carlo runs.

additional excess evaporation, but accentuated by outgassing during the same period. Most of the observed TA seasonal cycle is explained by the *E–P* term, leaving a biological TA drawdown to compensate for the largely positive inputs from physical transport over a year.

3.1.6. NCP and NCC

Figure 6 displays the seasonal cycle in NCP and NCC contributions to DIC and TA changes, the two processes that compose the biological term.

The ocean at Station ALOHA is net autotrophic over the annual mean, with NCP close to zero between October and February, and relatively consistent net autotrophy (DIC loss) of about 7 mmol mo^{-1} between March and September (data not shown). The cumulative average DIC (aNCP) loss from NCP is 1.2 ± 2.8 mol m^{-2} (Figure 6c).

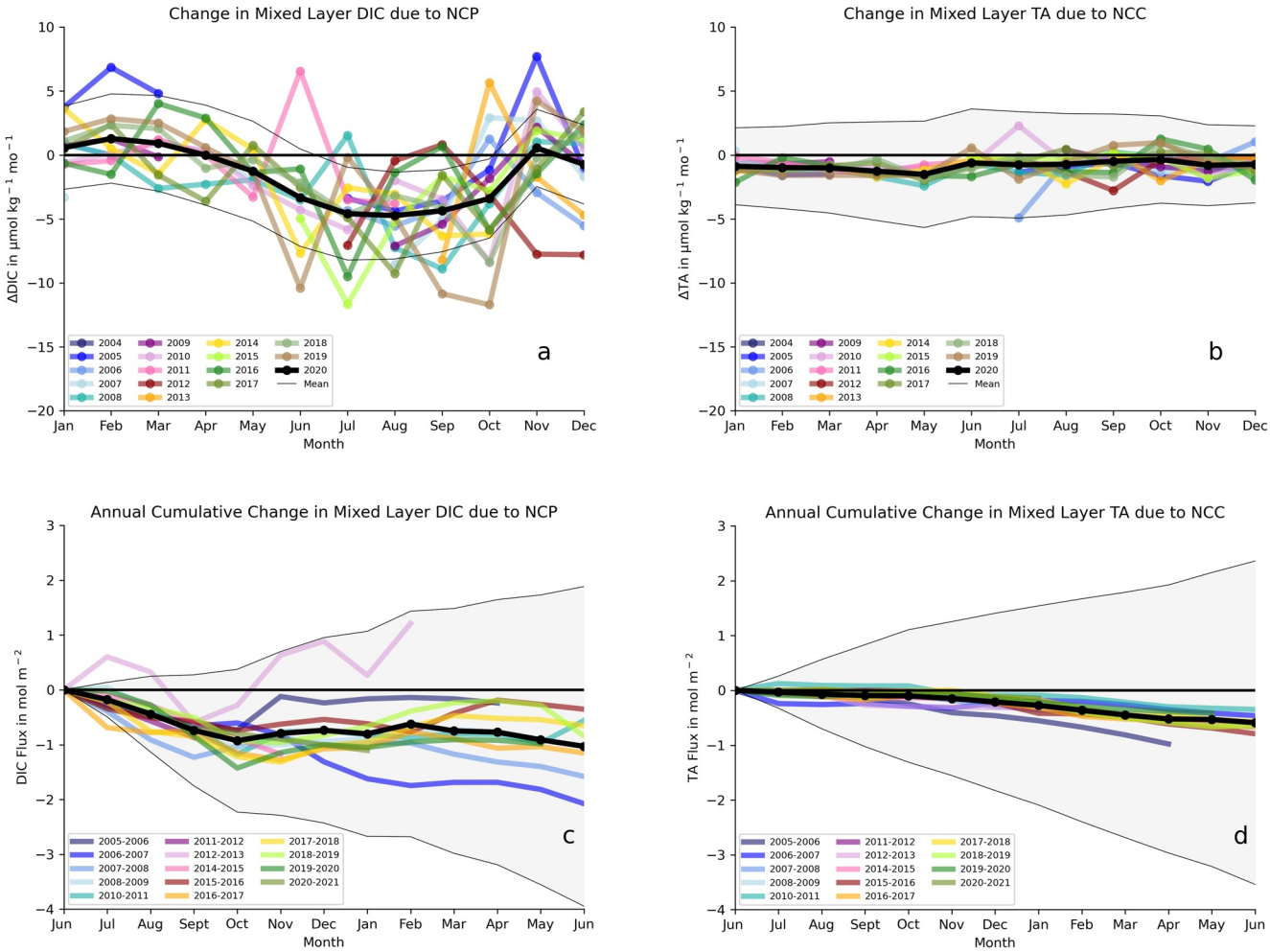

Figure 6. Yearly climatology of mixed layer NCP and NCC rates (6a, 6b), and (cumulative) aNCP and aNCC (6c, 6d) as well as averages for each year. Shaded area represents ±1 standard deviation of Monte Carlo runs. Only complete years shown for 6c and d.

TA drawdown from net calcification largely occurs in the winter and spring, between December and April, with values close to zero in the remaining months yielding net calcification (TA loss) over a year (Figure 6b). Cumulative NCC (aNCC) was 0.5 ± 2.7 mol m^{-2} of TA drawdown (Figure 6d).

3.2. Interannual Variability

The physical transport and *E-P* terms cannot be evaluated for interannual variability as the horizontal transport component and the diffusive flux for both TA/DIC and salinity are based on seasonal climatologies. Since the whole gas exchange term is resolved at hourly frequency, we can calculate true monthly averages of this term, enabling evaluation not just of seasonal climatology but also of changes from monthly to interannual time scales. High confidence in the monthly mean values is confirmed by the small variance between Monte Carlo runs (see Figure 3a). The cumulative DIC change due to gas exchange is positive for each complete deployment year (June to June). An exception is the strong El Niño year 2015–2016, where an intense outgassing period in August and September 2015 (Figure 7a, light green) yields a 2015–2016 DIC change from gas exchange that is virtually indistinguishable from zero (Figure 7b, yellow).

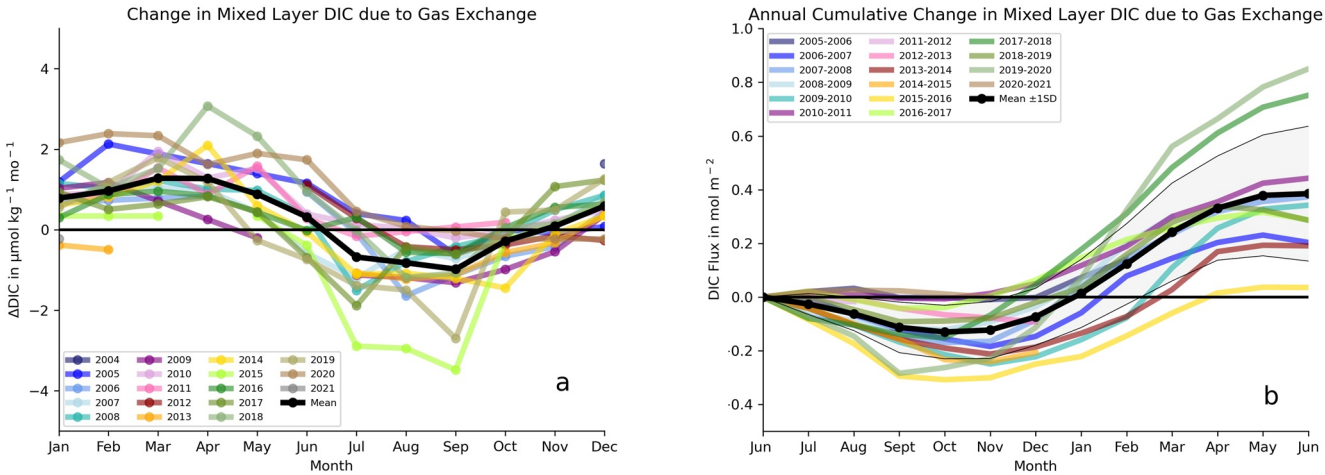

Figure 7. Change in mixed layer dissolved inorganic carbon due to gas exchange, both monthly averages in concentration change (7a), and total cumulative inputs over a year in mol C (7b).

4. Discussion

4.1. Annual NCP and NCC

Results of this study are on the lower end of the reported range for aNCP at this location (1.2 vs. mean 2.0 mol m^{-2}, see Table 5). However, given the error estimates here and in previous studies, none of the aNCP estimates are significantly different from the results presented here (see Table 5). In contrast, average aNCC is four to seven times larger than HOT sediment trap results, which constitute the only available data set with which to compare (Table 6). Sediment traps are known to provide a lower-end estimate for Particulate Inorganic Carbon (PIC) and Particulate Carbon (PC) export fluxes, but an inorganic carbon flux making up 50% of total carbon export is likely to be an overestimation at this site.

4.2. Discrepancies and Sensitivity Tests

A sensitivity analysis investigating different methodologies to quantify most of the terms of this carbon budget can shine a light on the origins of and insights from the divergence we see in average aNCP, and especially aNCC values compared to previous reports. The alternative methods used for E–P, horizontal transport, and diffusion terms are listed in Table 1 and expanded upon in the Supporting Information S1. Figure 8 shows NCP and NCC calculated using these methods.

4.2.1. Horizontal Transport

Data availability for horizontal gradients and eddy diffusivity still restricts us to a *seasonal* budget. The effect of using a time-varying current speed climatology instead of average current speeds to constrain horizontal transport illustrates a basic problem with using a seasonal budget approach at this location, where seasonality explains only a small fraction of the variability. As discussed in the methods section, current speeds at this location are dominated by mesoscale eddies, and also do not vary strongly with season at Station ALOHA (see Figure S3.2 in Supporting Information S1).

For a sensitivity check, using a current speed climatology from WHOTS ADCPs, instead of the average current speed used in Method A, drastically changes the horizontal transport term for TA and DIC (Figure S4 in Supporting Information S1), and consequently also NCC and NCP (Figure 7b). This is mainly based on the average direction of transport for individual months of the current climatology (Figure S2 in Supporting Information S1). However, this average direction does not represent any "real" seasonality in current speed and direction, as the currents have been shown to have no significant seasonality (Figure S3 in Supporting Information S1)—so the seasonality of the modified advective term is questionable. At locations of previous studies using this approach (Fassbender et al., 2016, 2017), horizontal contributions to the overall carbon budget were negligible or small compared to other budget components. Due to a much smaller contribution of vertical mixing and entrainment, at this location, the advective term becomes the most important physical transport process (Figure 4). It is therefore

Table 5
Literature Comparison of Average NCP Rates and aNCP Values at Station A Long-Term Oligotrophic Habitat Assessment

Study	Method	Time	Depth	aNCP (- mol C m^{-2} yr^{-1})	(mean) NCP rate (- mmol C m^{-2} d^{-1})
Emerson et al. (2008) [a]	O_2/Ar budget	2004–2005	ML	−4.2 ± 1.9	−11.5 ± 5.2
Keeling et al. (2004)	Diagnostic box model (DIC & $\delta^{13}C$)	1988–2002	ML	−2.2 ± 0.8	−6.0 ± 2.2
Lee (2001) [a]	DIC change	Summer 1990	ML	−2.3 ± 0.8	−6.3 ± 2.2
Quay et al. (2009) [a]	Carbon budget (DIC & $\delta^{13}C$)	2004–2005	ML	−2.4 ± 1.0	−7.85 ± 2.19
Quay et al. (2010) [a]	O_2/Ar budget	2006–2007	ML	−3.7 ± 1.0	−10.1 ± 2.7
Quay and Stutsman (2003)	Carbon budget (DIC & $\delta^{13}C$)	1994–1999	ML	−2.3 ± 1.3	−6.3 ± 3.4
Wilson et al. (2015)	Prior O_2/Ar-NCP	Jul-12	ML	-	−6.0 ± 3.2
Wilson et al. (2015)	Prior O_2/Ar-NCP	Aug-12	ML	-	7.6 ± 4.2
Wilson et al. (2015)	Prior O_2/Ar-NCP	Aug—Sep 2012	ML	-	0.5 ± 3.1
Sonnerup et al. (2013) [a]	CFC/SF_6 model	2008	Winter ML	−2.5 ± 3.0	−6.8 ± 8.2
Yang et al. (2017) [a]	O_2 budget	2014–2018	Winter ML	−2.4 ± 0.6	−6.6 ± 1.6
Emerson et al. (1995) [a]	O_2/Ar/N_2 budget	1990	0–100m	−1.0 ± 0.7	−2.7 ± 1.9
Emerson et al. (1997) [a]	O_2/Ar/N_2 budget	Early 1990s	0–100m	−2.7 ± 1.7	−7.4 ± 4.7
Sonnerup et al. (1999)	CFC model	1991	0–100m	−2.2 ± 0.5	−6.0 ± 1.4
Hamme and Emerson (2004)	O_2/Ar/N_2 budget	2000–2001	0–115m	−1.1 ± 0.5	−3.0 ± 1.4
Benitez-Nelson et al. (2001)	$^{234}Th/^{238}U$ disequilibrium	1999–2000	0–150m	−1.5 ± 0.8	−4.0 ± 2.3 (PC flux)
Brix et al. (2006)	Diagnostic box model (DIC & $\delta^{13}C$)	1989–2000	0–150m	−3.1 ± 0.3	−8.5 ± 0.8
Ferrón et al. (2021)	O_2/Ar	2014–2018	0–150m	−1.5 ± 0.4	−4.1 ± 1.1
Riser and Johnson (2008) [a]	O_2 budget	2002–2005	0–150m	−1.6 ± 0.2	−4.4 ± 0.5
Emerson (2014)	Average of literature values	-	-	−2.5 ± 0.7	−6.8 ± 1.9
This study	***Carbon budget (DIC & TA), Method A***	***2005–2021***	***ML***	***−1.2 ± 2.8***	***−2.0 ± 7.8***

[a]Adapted From Ferrón et al. (2021)

likely that the discrepancy between NCP & NCC calculated here and literature values can partly be explained by the lack of seasonality in this important transport term.

This illustrates the need for data on horizontal gradients of surface carbonate chemistry parameters at higher spatiotemporal resolution, as will hopefully be achieved by promising current and future endeavors using floats, autonomous vehicles, and satellites (e.g., Nicholson et al., 2022; Nickford et al., 2022). Recent time-varying 1° × 1° CO_2-carbonate chemistry products have become available at a monthly resolution, for example, Global Ocean Surface Carbon (GOSC; Chau et al., 2022) or OceanSODA-ETHZ (Gregor & Gruber, 2021). Unfortunately, these products currently do not capture variability at our study site (see Supporting Information S1, Figure S6 in Supporting Information S1) and to resolve eddy contributions, a finer spatial resolution is needed. With data on variability in TA/DIC gradients at the spatiotemporal scale of mesoscale eddies, the construction of a carbon budget at the appropriate time scale(s) would be possible, and the variable contributions of horizontal transport for carbon cycling at this location could be investigated.

4.2.2. Vertical Transport

For the vertical transport term, a heat budget based on Cronin et al. (2015) was constructed to constrain eddy diffusivity in a different way (see Supporting Information S1 and Table S2 in Supporting Information S1). Since there are order of magnitude differences in the climatological diffusivity values generated by the Keeling et al. (2004) and the Cronin et al. (2015) approaches, a sensitivity analysis to the choice of diffusivity coefficients was performed. Generally, due to increasing DIC with depth (a positive vertical DIC gradient), higher K_z will lead to increased diffusive DIC fluxes into the mixed layer, which, in turn, propagates to a larger biological term and more DIC drawdown from NCP (essentially balancing higher K_z input values). For TA, the relationship is less straightforward due to an alkalinity maximum associated with the

Table 6
Literature Comparison of Average Carbonate Fluxes at Station A Long-Term Oligotrophic Habitat Assessment in Different Units

Study	Term	Value	Units
Karl et al. (2021)	Average HOT PIC flux 2001–2019	24.2	mg CaCO3 m^{-2} d^{-1}
		2.9	mg C m^{-2} d^{-1}
Dong et al. (2019)	CaCO3 flux near ALOHA @100 m depth	71.1	mg CaCO3 m^{-2} d^{-1}
		8.5	mg C m^{-2} d^{-1}
Betzer et al. (1984)	Pteropod (aragonite) fluxes at 100 m. 21°N, Western North Pacific	32.6	mg CaCO3 m^{-2} d^{-1}
		3.9	mg C m^{-2} d^{-1}
Sabine et al. (1995)	Carbonate flux from dissolution	40	mg CaCO3 m^{-2} d^{-1}
		4.8	mg C m^{-2} d^{-1}
Sabine and Mackenzie (1995)	Sediment trap CaCO3 flux—HOT-7 200 m	40.3	mg CaCO3 m^{-2} d^{-1}
		4.8	mg C m^{-2} d^{-1}
Sabine and Mackenzie (1995)	Sediment trap CaCO3 flux—HOT-9 200 m	40.7	mg CaCO3 m^{-2} d^{-1}
		4.8	mg C m^{-2} d^{-1}
Sabine and Mackenzie (1995)	Sediment trap CaCO3 flux—HOT-11 200 m	39.4	mg CaCO3 m^{-2} d^{-1}
		4.7	mg C m^{-2} d^{-1}
Sabine and Mackenzie (1995)	Sediment trap CaCO3 flux—HOT-15 200 m	40.8	mg CaCO3 m^{-2} d^{-1}
		4.9	mg C m^{-2} d^{-1}
This study	**Mean mixed layer TA change from NCC**	**180 ± 190**	**mg CaCO3 m^{-2} d^{-1}**
		21.6 ± 22.8	**mg C m^{-2} d^{-1}**

North Pacific Tropical Water (NPTW) at Station ALOHA that varies in location relative to the mixed layer (Lukas & Santiago-Mandujano, 2008). Both time-varying K_z estimates show a peak in diffusive transport in the spring, and the shape of the annual cycles is remarkably similar, but they differ by an order of magnitude across their whole range (Figure S5 in Supporting Information S1). The Keeling et al. (2004) data is more in line with literature data, and the calculation based on the heat budget yields (unrealistic) negative values indicating up-gradient transport in the fall. As Figure 8 shows, the choice of K_z values strongly impacts the final NCP and NCC results, especially in the springtime when biological drawdown of DIC is most prevalent. Therefore, more measurements and refined budget calculations using float and mooring data to constrain K_z values at various temporal and spatial scales would be very useful for biogeochemical tracer budgets such as this one.

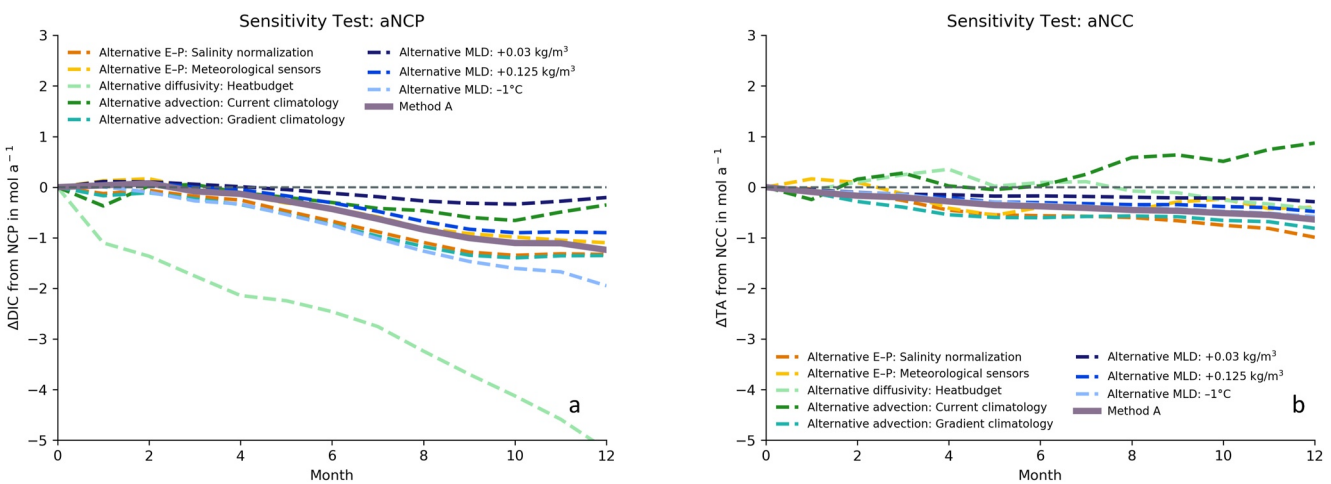

Figure 8. The sensitivity test for all different methodologies showing the resulting Monte Carlo average aNCP (8a) and aNCC (8b).

4.2.3. Evaporation—Precipitation

E–P using a salinity budget (Method A) versus salinity normalization is very similar, while the calculation based on WHOTS measurement yields much smaller fluxes (Figures S4 and S5 in Supporting Information S1). They all converge on (maximum) net evaporation during the summer/fall between June and October. With the direct calculation from mooring sensors, net evaporation persists throughout the year, while the other two approaches largely indicate net precipitation earlier in the year (Feb-May). The large discrepancy between the salinity-based and the directly measured approaches can be partly explained by rainfall measurements. Mooring precipitation sensors do not match satellite, shipboard, or model results largely because of the extreme patchiness of rainfall.

However, it is also likely that unresolved advective processes affect the salinity-based calculation, but that those contributions are canceled out in the final carbon budget. The residual of the salinity budget contains all errors and fluxes that are not accounted for in the physical transport terms. E–P is the residual of the salinity budget and appears to be driving most of the observed salinity variations; this suggests an underestimation of physical transport terms, as local precipitation and evaporation are not expected to be the main control of sea surface salinity. We assume that any unresolved processes affecting salinity are essentially conservative mixing processes (i.e., they affect TA and DIC proportionally), such as advection of regional gradients in salinity (and TA, DIC) from local precipitation differences that are not captured by $1° \times 1°$ climatological fields. Consequently, the use of the salinity budget for the E–P term is beneficial for the final carbon mass balance. Since the (scaled) salinity physical transport term is subtracted from the DIC/TA physical transport terms, any biases that they both exhibit should cancel out, similarly as discussed in Fassbender et al. (2016, Equation 10). While this shows again that the physical transport term taken alone is likely not resolving important contributions, this increases the confidence in the final NCC and NCP values.

4.2.4. Mixed-Layer Depth

Several definitions of MLD have been used at Station ALOHA, including the density criteria of +0.03 kg m^{-3} from De Boyer Montégut et al. (2004) (e.g., Barone et al., 2019; Ferrón et al., 2021; Karl et al., 2021), and +0.125 kg m^{-3} from Levitus (1982) (e.g., Dore et al., 2003, 2009, 2014; Quay & Stutsman, 2003; Wilson et al., 2015), as well as the temperature criterion of −1°C from Hastenrath & Merle (1987) (e.g., Cortés et al., 2001; Venrick, 1993). All MLD criteria yield very similar NCC estimates. While the general shape of the seasonal DIC changes from NCP is the same for all MLD estimates, the magnitude of these fluxes varies more between different estimates, leading to differences in cumulative aNCP from 0.25 mol C m^{-2} using the +0.03 kg m^{-3} density criterion (shallower ML definition) to ∼2 mol C m^{-2} using a −1°C temperature threshold (deeper ML definition). Although all of these estimates are within the aNCP error, this illustrates the importance of MLD definition for mixed layer carbon budgets.

It is worth mentioning that discrepancies between multiple approaches to some of these terms could only be exposed due to the unusual abundance of various complementary and redundant datasets at Station ALOHA, and could have easily gone unnoticed in other locations with less available data. There are issues with constraining seasonal fluxes of several key contributors to the carbon budget at this location compared to other studies, but the challenges adapting this approach are interesting results themselves: At Station ALOHA, where seasonal changes in MLD and stratification are much smaller than in the temperate ocean, constraints on (horizontal) transport from mesoscale eddies at the appropriate spatial resolution become a crucial ingredient for an accurate mixed layer carbon budget, and depending on the MLD definition, NCP can differ by a factor of 10. Additionally, and nonetheless, valuable insights can be gained from the budget components and final aNCC/aNCP estimates obtained from the most reliable (Method A) combination of methodologies, including a comparison of identified drivers of the seasonal carbon cycle and their relative contributions and timing to previously published studies.

4.3. Drivers of the Seasonal Carbon Cycle

In a recent study on net community production at Station ALOHA from oxygen dynamics, Ferrón et al. (2021) reported lower NCP rates between December and February, followed by an increase through June and then mostly high values (i.e., net autotrophy) through November. In this study, the NCP increase starts later, from April-June, and we observe a shift to near-zero NCP by October. Ferrón et al. (2021) suggest that their NCP_{ML} values in the late fall might be too high and suggest correcting for entrainment diffusive fluxes of oxygen by up to 65%–100% for individual months between Sep-Nov, which would lead to a 12% reduction in their aNCP estimate from 1.5 to 1.3 mol C, and thus bring that closer to the one presented here (1.2 ± 2.8 mol C).

There is agreement that the largest seasonal DIC signal at Station ALOHA is a summer drawdown of (salinity normalized) DIC due to biological activity (e.g., Keeling et al., 2004; Quay & Stutsman, 2003). However, the amplitude of this seasonal DIC drawdown is thought to be dampened because gas exchange is strongest around the same time but acts in the opposite direction: The air to sea flux is highest in spring (around April) when NCP strongly decreases mixed-layer DIC (Keeling et al., 2004). This hypothesis is largely confirmed by this study, with a small difference in timing. Maximum ingassing occurs in March-April, at 1–2 μmol kg^{-1} DIC mo^{-1}, and maximum drawdown from NCP occurs in May-August (Figure 6a). This is consistent with a peak in primary productivity later in the spring due to increased light and nutrient availability (from deepening PAR attenuation and a shoaling nutricline), and potential contribution from nitrogen-fixing cyanobacteria that are known to bloom with increasing stratification in the late summer (e.g., Karl & Church, 2017). Later in the summer, the continued biological DIC drawdown from NCP is enhanced by outgassing of DIC, but dampened by excess evaporation and increased physical transport inputs.

The main process that counteracts the spring-summer (biological) DIC drawdown here is physical transport, specifically lateral fluxes. Previous studies that utilized carbon budget models at Station ALOHA either constrained vertical diffusive fluxes and inferred horizontal transport (Keeling et al., 2004) or vice versa (Quay & Stutsman, 2003), with results varying considerably based on these assumptions. According to Keeling et al. (2004), the main processes behind mixed layer DIC variability are biological productivity, gas exchange and horizontal transport, as well as a period of winter entrainment. Quay and Stutsman (2003), on the other hand, stressed the importance of vertical diffusive fluxes supplying DIC to the mixed layer. This study concludes that the horizontal transport due to background advection and lateral eddy transport of DIC and TA plays a much larger role than vertical (entrainment and diffusion) or gas exchange fluxes over a year. The annual cycle in physical transport components shows advective DIC and TA loss especially in the early spring (DIC) and summer (TA), driven by a small zonal component of the gradient, with both parameters increasing to the west. Interestingly, previous studies have neglected zonal transport due to the small gradients (e.g., Dore et al., 2009; Keeling et al., 2004). Indeed, meridional gradients in DIC and TA are much steeper throughout the year, with both parameters increasing northward (see Supporting Information S1, Figures S3c and S3d in Supporting Information S1). However, the weak mean meridional flow (average 0.008 m s^{-1}) contributes only a small loss, and the net advective term is dominated by the stronger mean zonal flow acting on the (small) seasonally varying zonal gradient.

The annual CO_2 invasion here is 0.34 mol m^2. This estimate is lower than previous estimates based on pCO_2 calculated from discrete TA and DIC measurements (e.g., Quay and Stutsman (2003): 0.6 ± 0.4 mol C m^{-2}, Dore et al. (2009): ∼0.5 mol C m^{-2}), and underway pCO_2 data (Takahashi et al., 2009) but equivalent to earlier estimates from the WHOTS mooring (Sutton et al., 2017). A discrepancy between WHOTS flux estimates and underway pCO_2 systems was previously reported as 60% and was explained partly by differences in wind speed parameterization (Sutton et al. (2017)). Additionally, there is an average offset of about 8 μatm in measured pCO_2 at the WHOTS mooring compared to calculated pCO_2 from HOT measurements, which is small (2% of the mean) but grows considerably when integrated over time, such as in annual flux calculations. Possible contributors to this offset include differences in temperature (and therefore pCO_2) due to measuring depth (<1 m for WHOTS, 5–30 m for discrete data), conditions within the mooring measurement apparatus (equilibrator) not representing mean mixed layer pCO_2, or a systematic underestimation of pCO_2 calculated from TA & DIC, which has uncertainties of ±25 μatm (Orr et al., 2018). For this budget, both underestimated ingassing in the spring/summer and overestimated outgassing in the fall would entail underestimated NCP rates for these same months, and could be a reason for the relatively low aNCP reported here. Additionally, since for this budget CO_2 invasion is converted to a concentration change over the mixed layer, the choice in MLD definition also impacts the DIC *concentration* change, although it does not change the absolute amount of CO_2 taken up. A shallower mixed layer thus accentuates both outgassing and ingassing signals (see Figure S4b in Supporting Information S1).

Studies on calcium carbonate production and dissolution at Station ALOHA and in the NPSG are relatively sparse. Some studies in the 1980s and 1990s (e.g., Betzer et al., 1984; Sabine et al., 1995; Sabine & Mackenzie, 1995). Sabine and Mackenzie (1995) reported an export of around 40 mg $CaCO_3$ m^{-2} d^{-1}, and interestingly first detected the presence of calcium carbonate particles from benthic, more soluble calcifying organisms living on shallow, near-coastal banks in the water column at this location. To our knowledge, so far there have been no attempts to quantify seasonal variability in calcification/dissolution and $CaCO_3$ export dynamics at Station ALOHA. Cortés et al. (2001) studied the ecology of coccolithophores, an important calcifying phytoplankton and found extremely low abundances throughout most of the year. Only during March

and September/October, a fairly specific range of environmental conditions regarding temperature (20–25°C), salinity (34.9–35.2), nutrients (0.004–0.07 μmol/kg nitrate, <0.025 μmol/kg phosphate), and light availability (2-25 μE m^{-2} s^{-1}) appears to enable higher cell densities (Cortés et al., 2001). Only a very small fraction of zooplankton at Station ALOHA was reported to be made up of shelled pteropods (Steinberg et al., 2008), but they are likely a significant contributor to PIC exports due to their large size. Foraminifera, calcifying zooplankton, were examined by Monteagudo (2016) using bottom-moored sediment traps, and found to be more abundant during the summer months. Boeuf et al. (2019) investigated the species composition of particles retained in deep sea sediment traps and found foraminifera to be sporadically present in large concentrations, and pteropods generally abundant in deep sea particles. The sparse information on these three most important groups of calcifying organisms illustrates the highly variable nature of PIC export at Station ALOHA for each of them, highlighting the need for more species-specific studies of these organisms and the drivers of associated export events.

4.4. Interannual Variability

For both DIC and TA, interannual variability is much larger than the amplitude of a seasonal cycle, with a variance in monthly averages of about 30–50 μmol kg^{-1} between years, but an average seasonal cycle of only about 15 μmol kg^{-1}. All budget components evaluated here, including NCP and NCC, also vary on interannual time scales, with long-term changes likely exceeding the seasonal cycle in many cases. Multiple studies suggested that a strong influence of horizontal advection on both observed DIC and NCP exists at Station ALOHA on longer time scales. Yasunaka et al. (2014) associate DIC anomalies with changes in horizontal advection and MLD across the North Pacific. Brix et al. (2004) suggest that warmer years at Station ALOHA have both reduced lateral DIC transport, and diminished atmospheric uptake, leading to negative DIC anomalies, and suggesting that horizontal transport is a major DIC source for this location. They also found that interannual variations in NCP were largely associated with changes in horizontal transport of DIC, and hypothesize that enhanced lateral transport of DIC coincides with enhanced horizontal nutrient supply (Brix et al., 2004). This leads to a stronger biological drawdown of DIC when there are larger horizontal DIC inputs, which suggests that vertical processes play only a minor part in interannual NCP variability (Brix et al., 2004). Over an average year in this study, times of large horizontal DIC fluxes do not correspond to elevated NCP, showing that these processes are not coupled in the same way on a seasonal time scale. However, we do confirm that horizontal transport is the main process supplying both DIC and TA to the mixed layer.

5. Summary and Outlook

This study is the first attempt to quantify seasonality in calcification/dissolution dynamics at Station ALOHA, and results show annual net calcification of 0.5 ± 2.7 mol m^{-2}. This exceeds all previously reported fluxes from sediment trap data, with maximum export occurring during December-April.

The mixed layer ecosystem at Station ALOHA is confirmed to be net autotrophic over a year at about 1.2 ± 2.8 mol C m^{-2}. NCP during March-September exceeds the inputs from physical transport and CO_2 invasion, creating a distinct biological spring-summer DIC drawdown. The main supply of DIC to the mixed layer comes from horizontal transport throughout the year, with an additional distinct fall-winter peak from entrainment and consistent smaller diffusive fluxes. Contributions to DIC changes from evaporation and precipitation and gas exchange show clear opposing seasonal cycles. Lateral DIC fluxes are identified as the largest annual source of DIC to the mixed layer, resolving long-standing disagreements from studies on the importance of horizontal versus vertical transport terms.

At Station ALOHA, it would be particularly beneficial to resolve more than the annual cycle of carbon parameters, as variability on other time-scales is large compared to seasonal variations. This would require, most urgently, a data set constraining regional horizontal gradients in alkalinity and DIC at near-monthly time scales and mesoscale spatial scales, as could potentially be developed from algorithms employing satellite data as well as regional-scale ocean models. This could help remedy current errors on the order of 200% for aNCP and aNCC values and provide insights into carbonate system variability on other important time scales.

Data Availability Statement

Data obtained via the Hawaii Ocean Time-series HOT-DOGS application; University of Hawai'i at Mānoa. National Science Foundation Award # 175651 at https://hahana.soest.hawaii.edu/hot/hot-dogs/interface.html (HOT-DOGS (2022); Lukas et al. (2001)). WHOTS and MOSEAN mooring pCO_2, SST and salinity data are

available at https://www.nodc.noaa.gov/ocads/oceans/Moorings/WHOTS_158W_23N.html (Sutton et al., 2012) and https://www.nodc.noaa.gov/ocads/oceans/Moorings/MOSEAN.html (Sabine et al., 2012). WHOTS subsurface CTD, ADCP and VMCM datasets can be found through OceanSITES Global Data Assembly Center at https://dods.ndbc.noaa.gov/thredds/catalog/data/oceansites/DATA/WHOTS/catalog.html (NOAA, 2014). Wind stress data is available through the APDRC ERDDAP server at http://apdrc.soest.hawaii.edu/erddap/griddap/hawaii_soest_a6ab_91f7_b38f.html (ERDDAP—Home Page, 2022). This study has been conducted using E.U. Copernicus Marine Service Information: https://doi.org/10.48670/moi-00047 (Global Ocean Surface Carbon, 2022).

Acknowledgments
Thank you to John Dore for thoughtful feedback on the first version of the manuscript, and to Eric Firing for frequent and thorough support with conceptual and practical challenges. Thanks to the crewmembers and scientists running the Hawaii Ocean Time-series over the last three decades, especially Dan Sadler for the carbonate system samples and measurements. The HOT program is supported by the National Science Foundation (current Grant OCE-1756517; AEW, P.I.). The WHOI Hawaii Ocean Timeseries Station (WHOTS) is supported by the National Oceanic and Atmospheric Administration (NOAA) Global Ocean Monitoring and Observing Program through the Cooperative Institute for the North Atlantic Region (CINAR) under Cooperative Agreement NA14OAR4320158. NOAA CPO FundRef number (100007298). Subsurface measurements are supported by NSF as part of the Hawaii Ocean Timeseries (HOT) through Grants OCE-752606, 0926766, 1260164, and 1756517. We acknowledge the financial support of our research provided in part by a grant/cooperative agreement from the National Oceanic and Atmospheric Administration, CMAR award # NA21NMF4320043. The views expressed herein are those of the author(s) and do not necessarily reflect the views of NOAA or any of its subagencies. There are no perceived financial or other conflicts of interest for any author. This is SOEST contribution number 11689, and PMEL contribution number 5449.

References

Anderson, L., & Sarmiento, J. (1994). Redfield ratios of remineralization determined by nutrient data analysis. *Global Biogeochemical Cycles*, *8*(1), 65–80. https://doi.org/10.1029/93gb03318

Barone, B., Coenen, A. R., Beckett, S. J., Mcgillicuddy, D. J., Jr., Weitz, J. S., & Karl, D. M. (2019). The ecological and biogeochemical state of the North Pacific Subtropical Gyre is linked to sea surface height. *Journal of Marine Research*, *77*(2), 215–245. https://doi.org/10.1357/002224019828474241

Benitez-Nelson, C., Buesseler, K. O., Karl, D. M., & Andrews, J. (2001). A time-series study of particulate matter export in the North Pacific subtropical Gyre based on ^{234}Th: ^{238}U disequilibrium. *Deep Sea Research Part I: Oceanographic Research Papers*, *48*(12), 2595–2611. https://doi.org/10.1016/s0967-0637(01)00032-2

Betzer, P. R., Byrne, R. H., Acker, J. G., Lewis, C. S., Jolley, R. R., & Feely, R. A. (1984). The oceanic carbonate system: A reassessment of Biogenic Controls. *Science*, *226*, 1074–1077.

Bittig, H., Steinhoff, T., Claustre, H., Fiedler, B., Williams, N., Sauzède, R., et al. (2018). Nutrient concentrations from T, S, and O2 data using Bayesian neural networks. *Frontiers in Marine Science*, *5*, 328.

Boeuf, D., Edwards, B. R., Eppley, J. M., Hu, S. K., Poff, K. E., Romano, A. E., et al. (2019). Biological composition and microbial dynamics of sinking particulate organic matter at abyssal depths in the oligotrophic open ocean. *Proceedings of the National Academy of Sciences of the United States of America*, *116*(24), 11824–11832.

Brix, H., Gruber, N., Karl, D., & Bates, N. (2006). On the relationships between primary, net community, and export production in subtropical gyres. *Deep-Sea Research II*, *53*(5–7), 698–717. https://doi.org/10.1016/j.dsr2.2006.01.024

Brix, H., Gruber, N., & Keeling, C. D. (2004). Interannual variability of the upper ocean carbon cycle at station ALOHA near Hawaii. *Global Biogeochemical Cycles*, *18*(4), GB4019. https://doi.org/10.1029/2004gb002245

Broullón, D., Pérez, F., Velo, A., Hoppema, M., Olsen, A., Takahashi, T., et al. (2019). A global monthly climatology of total alkalinity: A neural network approach. *Earth System Science Data*, *11*(3), 1109–1127. https://doi.org/10.5194/essd-11-1109-2019

Broullón, D., Pérez, F. F., Velo, A., Hoppema, M., Olsen, A., Takahashi, T., et al. (2020). A global monthly climatology of oceanic total dissolved inorganic carbon: A neural network approach. *Earth System Science Data*, *12*(3), 1725–1743. https://doi.org/10.5194/essd-12-1725-2020

Carter, B. R., Feely, R. A., Williams, N. L., Dickson, A. G., Fong, M. B., & Takeshita, Y. (2018). Updated methods for global locally interpolated estimation of alkalinity, pH, and nitrate. *Limnology and Oceanography: Methods*, *16*(2), 119–131. https://doi.org/10.1002/lom3.10232

Chau, T. T. T., Gehlen, M., & Chevallier, F. (2022). A seamless ensemble-based reconstruction of surface ocean pCO_2 and air–sea CO_2 fluxes over the global coastal and open oceans. *Biogeosciences*, *19*(4), 1087–1109. https://doi.org/10.5194/bg-19-1087-2022

Church, M. J., Lomas, M. W., & Muller-Karger, F. (2013). Sea change: Charting the course for biogeochemical ocean time-series research in a new millennium. *Deep-Sea Research II*, *93*, 2–15. https://doi.org/10.1016/j.dsr2.2013.01.035

Cortés, M. Y., Bollmann, J., & Thierstein, H. R. (2001). Coccolithophore ecology at the HOT station ALOHA, Hawaii. *Deep-Sea Research II*, *48*(8–9), 1957–1981. https://doi.org/10.1016/s0967-0645(00)00165-x

Cronin, M. F., Pelland, N. A., Emerson, S. R., & Crawford, W. R. (2015). Estimating diffusivity from the mixed layer heat and salt balances in the North Pacific. *Journal of Geophysical Research: Oceans*, *120*(11), 7346–7362. https://doi.org/10.1002/2015jc011010

De Boyer Montégut, C., Madec, G., Fischer, A. S., Lazar, A., & Iudicone, D. (2004). Mixed layer depth over the global ocean: An examination of profile data and a profile-based climatology. *Journal for Geophysical Research - Oceans*, *109*(C12), C12003. https://doi.org/10.1029/2004JC002378

Dickson, A. G. (1990). Standard potential of the reaction: AgCl(s) + 1/2H2(g) = Ag(s) + HCl(aq), and the standard acidity constant of the ion HSO4- in synthetic seawater from 273.15 to 318.15 K. *Journal of Chemical Thermodynamics*, *22*(2), 113–127. https://doi.org/10.1016/0021-9614(9090074-Z)

Dickson, A. G., & Riley, J. P. (1979). The estimation of acid dissociation constants in sea-water media from potentiometric titrations with strong base. II. The dissociation of phosphoric acid. *Marine Chemistry*, *7*(2), 101–109. https://doi.org/10.1016/0304-4203(79)90002-1

Dong, S., Berelson, W., Rollins, N., Subhas, A., Naviaux, J., Celestian, A., et al. (2019). Aragonite dissolution kinetics and calcite/aragonite ratios in sinking and suspended particles in the North Pacific. *Earth and Planetary Science Letters*, *515*, 1–12. https://doi.org/10.1016/j.epsl.2019.03.016

Dore, J., Church, M., Karl, D., Sadler, D., & Letelier, R. (2014). Paired windward and leeward biogeochemical time series reveal consistent surface ocean CO2 trends across the Hawaiian Ridge. *Geophysical Research Letters*, *41*(18), 6459–6467. https://doi.org/10.1002/2014gl060725

Dore, J., Lukas, R., Sadler, D., & Karl, D. (2003). Climate-driven changes to atmospheric CO2 sink in the subtropical North Pacific Ocean. *Nature*, *424*(6950), 754–757. https://doi.org/10.1038/nature01885

Dore, J. E., Lukas, R., Sadler, D. W., Church, M. J., & Karl, D. M. (2009). Physical and biogeochemical modulation of ocean acidification in the central North Pacific. *Proceedings of the National Academy of Sciences*, *106*(30), 12235–12240. https://doi.org/10.1073/pnas.0906044106

Emerson, S. (2014). Annual net community production and the biological carbon flux in the ocean. *Global Biogeochemical Cycles*, *28*(1), 14–28. https://doi.org/10.1002/2013GB004680

Emerson, S., Quay, P. D., Karl, D. M., Winn, C., Tupas, L., & Landry, M. (1997). Experimental determination of the organic carbon flux from open-ocean surface waters. *Nature*, *389*(6654), 951–954. https://doi.org/10.1038/40111

Emerson, S., Quay, P. D., Stump, C., Wilbur, D., & Schudlich, R. (1995). Chemical tracers of productivity and respiration in the subtropical Pacific Ocean. *Journal of Geophysical Research*, *100*(C8), 873–887. https://doi.org/10.1029/95jc01333

Emerson, S., Stump, C., & Nicholson, D. P. (2008). Net biological oxygen production in the ocean: Remote in situ measurements of O2 and N2 in surface waters. *Global Biogeochemical Cycles*, *22*(3), GB3023. https://doi.org/10.1029/2007GB003095

ERDDAP - Home Page. (2022). ERDDAP - Home page. [Dataset]. ERDDAP. Retrieved from https://apdrc.soest.hawaii.edu/erddap/index.html

Fassbender, A. J., Sabine, C. L., & Cronin, M. F. (2016). Net community production and calcification from 7 years of NOAA Station Papa Mooring measurements. *Global Biogeochemical Cycles*, *30*(2), 250–257. https://doi.org/10.1002/2015gb005205

Fassbender, A. J., Sabine, C. L., Cronin, M. F., & Sutton, A. J. (2017). Mixed-layer carbon cycling at the Kuroshio extension observatory. *Global Biogeochemical Cycles*, *31*(2), 272–288. https://doi.org/10.1002/2016gb005547

Fernández-Castro, B., Mouriño-Carballido, B., Benítez-Barrios, V. M., Chouciño, P., Fraile-Nuez, E., Graña, R., et al. (2014). Microstructure turbulence and diffusivity parameterization in the tropical and subtropical Atlantic, Pacific and Indian Oceans during the Malaspina 2010 expedition. *Deep Sea Research Part I: Oceanographic Research Papers*, *94*, 15–30. https://doi.org/10.1016/j.dsr.2014.08.006

Ferrón, S., Barone, B., Church, M. J., White, A. E., & Karl, D. M. (2021). Euphotic zone metabolism in the North Pacific Subtropical Gyre based on oxygen dynamics. *Global Biogeochemical Cycles*, *35*(3), e2020GB006744. https://doi.org/10.1029/2020GB006744

Global Ocean Surface Carbon. (2022). E.U. Copernicus Marine Service Information (CMEMS). [Dataset]. https://doi.org/10.48670/moi-00047

Gregor, L., & Gruber, N. (2021). OceanSODA-ETHZ: A global gridded data set of the surface ocean carbonate system for seasonal to decadal studies of ocean acidification. *Earth System Science Data*, *13*(2), 777–808. https://doi.org/10.5194/essd-13-777-2021

Hamme, R. C., & Emerson, S. (2004). The solubility of neon, nitrogen and argon in distilled water and seawater. *Deep-Sea Research Part I Oceanographic Research Papers*, *51*(11), 1517–1528. https://doi.org/10.1016/j.dsr.2004.06.009

Hastenrath, S., & Merle, J. (1987). Annual cycle of subsurface thermal structure in the tropical Atlantic Ocean. *Journal of Physical Oceanography*, *17*(9), 1518–1538. https://doi.org/10.1175/1520-0485(1987)017<1518:acosts>2.0.co;2

Ho, D. T., Law, C., Smith, M., Schlosser, P., Harvey, M., & Hill, P. (2006). Measurements of air-sea gas exchange at high wind speeds in the Southern Ocean: Implications for global parameterizations. *Geophysical Research Letters*, *33*(16), L16611. https://doi.org/10.1029/2006gl026817

HOT-DOGS: the Hawaii Ocean Time-series Data Organization & Graphical System. (2022). [Dataset]. Retrieved from https://hahana.soest.hawaii.edu/hot/hot-dogs/interface.html

Humphreys, M. P., Lewis, E. R., Sharp, J. D., & Pierrot, D. (2022). PyCO2SYS v1.8: Marine carbonate system calculations in Python. *Geoscientific Model Development*, *15*(1), 15–43. https://doi.org/10.5194/gmd-15-15-2022

Humphreys, M. P., Schiller, A. J., Sandborn, D. E., Gregor, L., Pierrot, D., van Heuven, S. M. A. C., et al. (2022). *PyCO2SYS: Marine carbonate system calculations in Python*. Zenodo. https://doi.org/10.5281/zenodo.3744275

Karl, D., & Church, M. (2017). Ecosystem structure and dynamics in the North Pacific Subtropical Gyre: New views of an old ocean. *Ecosystems*, *20*(3), 433–457. https://doi.org/10.1007/s10021-017-0117-0

Karl, D., & Church, M. (2018). Station ALOHA: A gathering place for discovery, education, and scientific collaboration. *Limnology and Oceanography Bulletin*, *28*(1), 10–12. https://doi.org/10.1002/lob.10285

Karl, D. M., Christian, J. R., Dore, J. E., Hebel, D. V., Letelier, R. M., Tupas, L. M., & Winn, C. D. (1996). Seasonal and interannual variability in primary production and particle flux at Station ALOHA. *Deep Sea Research II*, *43*(2–3), 539–568. https://doi.org/10.1016/0967-0645(96)00002-1

Karl, D. M., Letelier, R. M., Bidigare, R. R., Björkman, K. M., Church, M. J., Dore, J. E., & White, A. E. (2021). Seasonal-to-decadal scale variability in primary production and particulate matter export at Station ALOHA. *Progress in Oceanography*, *195*, 102563. https://doi.org/10.1016/j.pocean.2021.102563

Karl, D. M., & Lukas, R. (1996). The Hawaii Ocean Time-series (HOT) program: Background, rationale and field implementation. *Deep Sea Research Part II: Topical Studies in Oceanography*, *43*(2–3), 129–156. https://doi.org/10.1016/0967-0645(96)00005-7

Keeling, C. D., Brix, H., & Gruber, N. (2004). Seasonal and long-term dynamics of the upper ocean carbon cycle at Station ALOHA near Hawaii. *Global Biogeochemical Cycles*, *18*(4), GB4006. https://doi.org/10.1029/2004gb002227

Kwon, Y. K., Primeau, F., & Sarmiento, J. L. (2009). The impact of remineralization depth on the air-sea carbon balance. *Nature Geoscience*, *2*(9), 630–635. https://doi.org/10.1038/ngeo612

Lee, K. (2001). Global net community production estimated from the annual cycle of surface water total dissolved inorganic carbon. *Limnology & Oceanography*, *46*(6), 1287–1297. https://doi.org/10.4319/lo.2001.46.6.1287

Letelier, R. M., Karl, D. M., Abbott, M. R., Flament, P., Freilich, M., Lukas, R., & Strub, T. (2000). Role of late winter mesoscale events in the biogeochemical variability of the upper water column of the North Pacific Subtropical Gyre. *Journal of Geophysical Research*, *105*(C12), 287723–328739.

Levitus, S. (1982). *Climatological atlas of the world ocean* (Vol. 13). US Department of Commerce, National Oceanic and Atmospheric Administration.

Liu, W. T., Katsaros, K. B., & Businger, J. A. (1979). Bulk parameterization of air-sea exchanges of heat and water vapor including the molecular constraints at the interface. *Journal of the Atmospheric Sciences*, *36*(9), 1722–1735. https://doi.org/10.1175/1520-0469(1979)036<1722:bpoase>2.0.co;2

Lukas, R., Church Matthew, J., Karl David, M., & University of Hawaii (2001). Physical and biochemical oceanographic data from the Hawaii Ocean Time-series (HOT) program collected by University of Hawaii at Station ALOHA in the Pacific Ocean 100 miles north of Oahu, Hawaii, since 1988 [Dataset]. NOAA National Centers for Environmental Information. https://www.ncei.noaa.gov/archive/accession/Station-ALOHA-HOT

Lukas, R., & Santiago-Mandujano, F. (2008). Interannual to interdecadal salinity variations observed near Hawaii: Local and remote forcing by surface freshwater fluxes. *Oceanography*, *21*(1), 46–55. https://doi.org/10.5670/oceanog.2008.66

Marinov, I., Follows, M., Gnanadesikan, A., Sarmiento, J. L., & Slater, R. D. (2008). How does ocean biology affect atmospheric pCO_2? Theory and models. *Journal of Geophysical Research*, *113*(C7), C07032. https://doi.org/10.1029/2007JC004598

Martínez-Moreno, J., Hogg, A. M., & England, M. H. (2022). Climatology, seasonality, and trends of spatially coherent ocean eddies. *Journal of Geophysical Research: Oceans*, *127*(7), e2021JC017453. https://doi.org/10.1029/2021JC017453

McLaughlin, K., Weisberg, S. B., Dickson, A. G., Hofmann, G. E., Newton, J. A., Aseltine-Neilson, D., et al. (2015). Core principles of the California Current Acidification Network: Linking chemistry, physics, and ecological effects. *Oceanography*, *28*(2), 160–169. https://doi.org/10.5670/oceanog.2015.39

Monteagudo, M. M. (2016). *Planktonic foraminiferal faunal study and Mg/Ca-temperature calibration at the Hawaii Ocean Time-Series*. University of California.

National Oceanic and Atmospheric Administration. (2014). Oceansites GDAC [Dataset]. NDBC DODS Server. Retrieved from https://dods.ndbc.noaa.gov/oceansites/

Neuer, S., Davenport, R., Freudenthal, T., Wefer, G., Llinás, O., Rueda, M.-J., et al. (2002). Differences in the biological carbon pump at three subtropical ocean sites. *Geophysical Research Letters*, *29*(18), 1885–1932-4. https://doi.org/10.1029/2002GL015393

Nicholson, S.-A., Whitt, D. B., Fer, I., du Plessis, M. D., Lebéhot, A. D., Swart, S., et al. (2022). Storms drive outgassing of CO_2 in the subpolar Southern Ocean. *Nature Communications*, *13*(1), 158. https://doi.org/10.1038/s41467-021-27780-w

Nickford, S., Palter, J. B., Donohue, K., Fassbender, A. J., Gray, A. R., Long, J., et al. (2022). Autonomous wintertime observations of air-sea exchange in the Gulf stream reveal a perfect storm for ocean CO2 uptake. *Geophysical Research Letters*, *49*(5), e2021GL096805. https://doi.org/10.1029/2021GL096805

Nightingale, P. D., Malin, G., Law, C. S., Watson, A. J., Liss, P. S., Liddicoat, M. I., et al. (2000). In situ evaluation of air-sea gas exchange parameterizations using novel conservative and volatile tracers. *Global Biogeochemical Cycles*, *14*(1), 373–387. https://doi.org/10.1029/1999gb900091

Orr, J. C., Epitalon, J. M., Dickson, A. G., & Gattuso, J. P. (2018). Routine uncertainty propagation for the marine carbon dioxide system. *Marine Chemistry*, *207*, 84–107. https://doi.org/10.1016/j.marchem.2018.10.006

Quay, P., & Stutsman, J. (2003). Surface layer carbon budget for the subtropical N. Pacific: $\delta^{13}C$ constraints at station ALOHA. *Deep-Sea Research Part I Oceanographic Research Papers*, *50*(9), 1045–1061. https://doi.org/10.1016/s0967-0637(03)00116-x

Quay, P. D., Peacock, C., Björkman, K., & Karl, D. M. (2010). Measuring primary production rates in the ocean: Enigmatic results between incubation and non-incubation methods at Station ALOHA. *Global Biogeochemical Cycles*, *24*, GB3014. https://doi.org/10.1029/2009GB003665

Quay, P. D., Stutsman, J., Feely, R. A., & Juranek, L. W. (2009). Net community production rates across the subtropical and equatorial Pacific Ocean estimated from air-sea δ13C disequilibrium. *Global Biogeochemical Cycles*, *23*(2), GB2006. https://doi.org/10.1029/2008GB003193

Riser, S. C., & Johnson, K. S. (2008). Net production of oxygen in the subtropical ocean. *Nature*, *451*(7176), 323–325. https://doi.org/10.1038/nature06441

Sabine, C., & Mackenzie, F. (1995). Bank-derived carbonate sediment transport and dissolution constraints at Station ALOHA in the Hawaiian archipelago. *Aquatic Geochemistry*, *1*(2), 189–230. https://doi.org/10.1007/bf00702891

Sabine, C. L., Mackenzie, F. T., Winn, C., & Karl, D. M. (1995). Geochemistry of carbon dioxide in seawater at the Hawaii Ocean Time series station, ALOHA. *Global Biogeochemical Cycles*, *9*(4), 637–651. https://doi.org/10.1029/95gb02382

Sabine, C. L., Maenner Jones, S., Bott, R., & Sutton, A. J. (2012). High-resolution ocean and atmosphere pCO2 time-series measurements from mooring MOSEAN_158W_23N (NCEI Accession 0100073) [Complete dataset]. [Dataset]. NOAA National Centers for Environmental Information. https://doi.org/10.3334/cdiac/otg.tsm_mosean

Santiago-Mandujano, F., Lukas, R., Murphy, D. J., & Larson, N. G. (2016). *MicroCAT/SeaCAT sensor calibration and data quality control: Lessons learned from 10 Years of WHOI-Hawaii Ocean Time-series site (WHOTS) mooring deployments* (pp. OD14C–2432). American Geophysical Union.

Sarmiento, J. L., & Gruber, N. (2006). Carbon cycle. In *Ocean biogeochemical dynamics* (pp. 318–391). Princeton University Press.

Sigman, D. M., & Boyle, E. A. (2000). Glacial/interglacial variations in atmospheric carbon dioxide. *Nature*, *407*(6806), 859–869. https://doi.org/10.1038/35038000

Sonnerup, R. E., Mecking, S., & Bullister, J. L. (2013). Transit time distributions and oxygen utilization rates in the Northeast Pacific Ocean from chlorofluorocarbons and sulfur hexafluoride. *Deep-Sea Research Part I Oceanographic Research Papers*, *72*, 61–71. https://doi.org/10.1016/j.dsr.2012.10.013

Sonnerup, R. E., Quay, P. D., & Bullister, J. L. (1999). Thermocline ventilation and oxygen utilization rates in the subtropical North Pa-cific based on CFC distributions during WOCE. *Deep-Sea Research Part I Oceanographic Research Papers*, *45*(5), 777–805. https://doi.org/10.1016/S0967-0637(98)00092-2

Sprintall, J., & Tomczak, M. (1992). Evidence of the barrier layer in the surface layer of the tropics. *Journal of Geophysical Research*, *97*(C5), 7305–7316. https://doi.org/10.1029/92jc00407

Steinberg, D. K., Cope, J. S., Wilson, S. E., & Kobari, T. (2008). A comparison of mesopelagic mesozooplankton community structure in the subtropical and subarctic North Pacific Ocean. *Deep Sea Research Part II: Topical Studies in Oceanography*, *55*(14–15), 1615–1635. https://doi.org/10.1016/j.dsr2.2008.04.025

Sulpis, O., Lauvset, S. K., & Hagens, M. (2020). Current estimates of K_1^* and K_2^* appear inconsistent with measured CO_2 system parameters in cold oceanic regions. *Ocean Science*, *16*(4), 847–862. https://doi.org/10.5194/os-2020-19

Sutton, A. J., Sabine, C. L., Dietrich, C., Maenner Jones, S., Musielewicz, S., Bott, R., & Osborne, J. (2012). High-resolution ocean and atmosphere pCO_2 time-series measurements from mooring WHOTS_158W_23N in the North Pacific Ocean (NCEI Accession 0100080) [Dataset]. NOAA National Centers for Environmental Information. https://doi.org/10.3334/cdiac/otg.tsm_whots

Sutton, A. J., Sabine, C. L., Feely, R. A., Cai, W. J., Cronin, M. F., McPhaden, M. J., et al. (2016). Using present-day observations to detect when anthropogenic change forces surface ocean carbonate chemistry outside preindustrial bounds. *Biogeosciences*, *13*(17), 5065–5083. https://doi.org/10.5194/bg-13-5065-2016

Sutton, A. J., Sabine, C. L., Maenner-Jones, S., Lawrence-Slavas, N., Meinig, C., Feely, R. A., et al. (2014). A high-frequency atmospheric and seawater pCO_2 data set from 14 open-ocean sites using a moored autonomous system. *Earth System Science Data*, *6*(2), 353–366. https://doi.org/10.5194/essd-6-353-2014

Sutton, A. J., Wanninkhof, R., Sabine, C. L., Feely, R. A., Cronin, M. F., & Weller, R. A. (2017). Variability and trends in surface seawater pCO_2 and CO_2 flux in the Pacific Ocean. *Geophysical Research Letters*, *44*(11), 5627–5636. https://doi.org/10.1002/2017GL073814

Takahashi, T., Sutherland, S. C., Wanninkhof, R., Sweeney, C., Feely, R. A., Chipman, D. W., et al. (2009). Climatological mean and decadal change in surface ocean pCO_2, and net sea–air CO_2 flux over the global oceans. *Deep Sea Research Part II: Topical Studies in Oceanography*, *56*(8-10), 554–577.

Uppström, L. R. (1974). The boron/chlorinity ratio of deep-sea water from the Pacific Ocean. *Deep-Sea Research*, *21*(2), 161–162. https://doi.org/10.1016/0011-7471(74)90074-6

Venrick, E. L. (1993). Phytoplankton seasonality in the Central North Pacific: The endless summer reconsidered. *Limnology & Oceanography*, *28*(6), 1135–1149. https://doi.org/10.4319/lo.1993.38.6.1135

Wanninkhof, R. (1992). Relationship between wind speed and gas exchange over the ocean. *Journal of Geophysical Research*, *97*(C5), 7373–7382. https://doi.org/10.1029/92jc00188

Weiss, R. (1974). Carbon dioxide in water and seawater: The solubility of a non-ideal gas. *Marine Chemistry*, *2*(3), 203–215. https://doi.org/10.1016/0304-4203(74)90015-2

Weller, R. A., & David, R. E. (1980). A vector measuring current meter. *Deep-Sea Research*, *27A*(7), 565–582. https://doi.org/10.1016/0198-0149(80)90041-2

Wilson, S., Barone, B., Ascani, F., Bidgare, R. R., Church, M. J., del Valle, D. A., et al. (2015). Short-term variability in euphotic zone biogeochemistry and primary productivity at station ALOHA: A case study of summer 2012. *Global Biogeochemical Cycles*, *29*(8), 1145–1164. https://doi.org/10.1002/2015gb005141

Winn, C. D., Li, Y. H., Mackenzie, F. T., & Karl, D. M. (1998). Rising surface ocean dissolved inorganic carbon at the Hawaii Ocean Time-series site. *Marine Chemistry*, *60*(1–2), 33–47. https://doi.org/10.1016/s0304-4203(97)00085-6

Winn, C. D., Mackenzie, F. T., Carrillo, C. J., Sabine, C. L., & Karl, D. M. (1994). Air-sea carbon dioxide exchange in the North Pacific Subtropical Gyre: Implications for the global carbon budget. *Global Biogeochemical Cycles*, *8*(2), 157–163. https://doi.org/10.1029/94gb00387

Yang, B., Emerson, S., & Bushinsky, S. M. (2017). Annual net community production in the subtropical Pacific Ocean from in situ oxygen measurements on profiling floats. *Global Biogeochemical Cycles*, *31*(4), 728–744. https://doi.org/10.1002/2016GB005545

Yasunaka, S., Nojri, Y., Nakaoka, S., Ono, T., Mukai, H., & Usui, N. (2014). North Pacific dissolved inorganic carbon variations related to the Pacific Decadal Oscillation. *Geophysical Research Letters*, *41*, 1005–1011. https://doi.org/10.1002/2013GL058987

Zhurbas, V., & Oh, I. S. (2004). Drifter-derived maps of lateral diffusivity in the Pacific and Atlantic Oceans in relation to surface circulation patterns. *Journal of Geophysical Research*, *109*(C5), C05015. https://doi.org/10.1029/2003jc002241

References From the Supporting Information

Denman, K. L., & Gargett, A. E. (1983). Time and space scales of vertical mixing and advection of phytoplankton in the upper ocean. *Limnology & Oceanography*, *28*(5), 801–815. https://doi.org/10.4319/lo.1983.28.5.0801